THE CASE FOR $d_{x^2-y^2}$ PAIRING IN THE CUPRATE SUPERCONDUCTORS

D.J. SCALAPINO

Department of Physics, University of California, Santa Barbara, CA 93106-9530, USA

ELSEVIER

AMSTERDAM – LAUSANNE – NEW YORK – OXFORD – SHANNON – TOKYO

ELSEVIER

Physics Reports 250 (1995) 329–365

PHYSICS REPORTS

The case for $d_{x^2-y^2}$ pairing in the cuprate superconductors

D.J. Scalapino

Department of Physics, University of California, Santa Barbara, CA 93106-9530, USA

Received July 1994; editor: D.L. Mills

Contents:

1. Introduction	331	Appendix A	356
2. Why might it happen?	334	Appendix B	359
3. How would we know?	343	References	361
4. Conclusions	354	Note added in proof	365

Abstract

The nature of the orbital structure of the pairs in the superconducting phase of the high-temperature superconducting cuprates remains one of the central questions in this field. Here we examine the possibility that the superconducting state of these materials is characterized by $d_{x^2-y^2}$ pairing. We begin by looking theoretically at why this type of pairing might be favored in a strongly correlated system with a short-range Coulomb interaction. Then we turn to the experimental question of how one would know if $d_{x^2-y^2}$ pairing were present.

SSDI 0370-1573(94)00086-7

1. Introduction

It has been eight years since Bednorz and Muller's paper [1] on "Possible High T_c Superconductivity in the Ba–La–Cu–O System" was published. During this time the transition temperature of the cuprate superconductors has risen [2] to 134 K in $HgBa_2Ca_2Cu_4O_{8+\delta}$, and there have been many experimental and theoretical studies of the remarkable properties of this class of materials [3–5]. At the present, there remain widely divergent views regarding the nature of both the normal and the superconducting states as well as the origin of the pairing mechanism [6]. Here we will take the view that spin-fluctuations play a central role in determining the physical properties of the cuprates and within this framework examine the case for $d_{x^2-y^2}$ pairing. Specifically, we will discuss two questions about the possibility of $d_{x^2-y^2}$ pairing: (1) Why might it happen? and (2) How would we know?

Before beginning, we note that the basic structure of the cuprates consists of CuO_2 sheets as shown for $La_{2-x}Sr_xCuO_4$ in Fig. 1. In the undoped $x = 0$ state, the Cu^{+2} ions are in a nominal $(3d)^9$ configuration and have a magnetic moment. Below a Neel temperature, as shown in the phase diagram [7] of Fig. 2, the undoped system is an insulating antiferromagnet with a charge transfer gap [8]. When Sr replaces some of the La, additional holes are added to the CuO_2 layer. As the system is doped with holes, the antiferromagnetic order is suppressed, and the system eventually becomes metallic and superconducting. The phase diagram of Fig. 2 also indicates that besides the insulating-metal crossover, there is a spin-glass-like region and an orthorhombic to tetragonal lattice transition.

With such a rich phase diagram, one can understand that there would be a variety of proposed pairing mechanisms and superconducting states. These include electron-phonon [9] or charge-transfer models [10] in which the orbital pairing state has s-wave or anisotropic s-wave symmetry, models

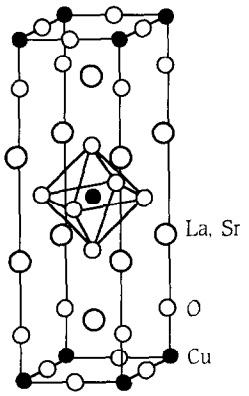

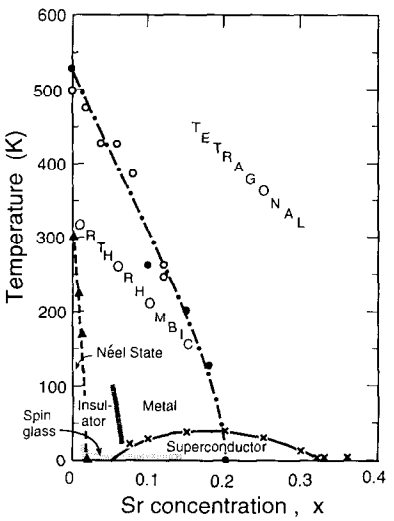

Fig. 1. The structure of La_2CuO_4. The CuO_2 sheets are believed to be the active region for pairing when additional holes are added by replacing some of the La with Sr (from Almasan and Maple [170]).

Fig. 2. Phase diagram of $La_{2-x}Sr_xCuO_4$ (from Keimer et al. [7]). The superconducting phase boundary for $x > 0.2$ remains under discussion [169,168].

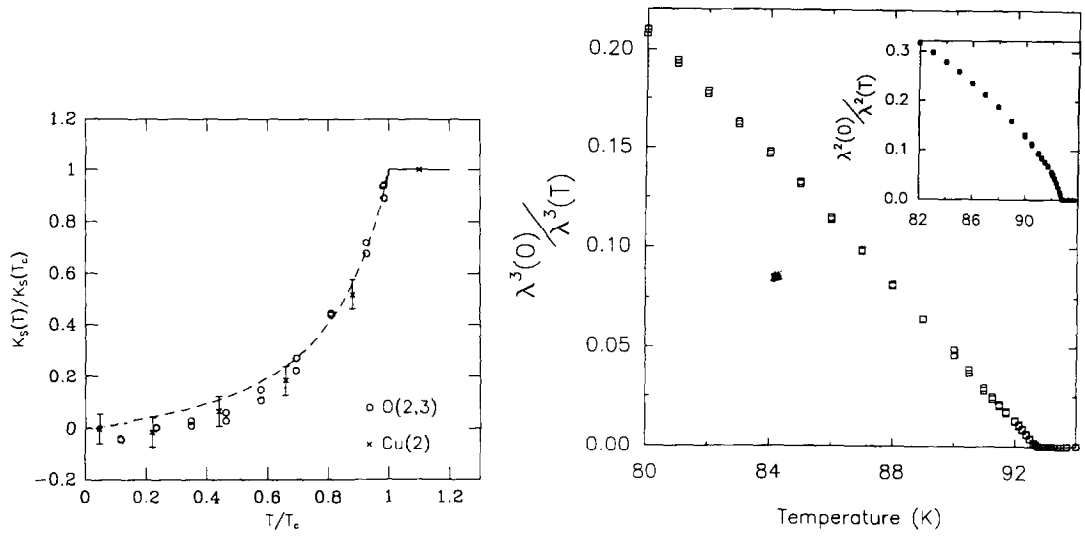

Fig. 3. Knight shift K versus reduced temperature for Cu (Barrett et al. [16]) and O (Takigawa et al. [17]). The dashed curve shows the result of a calculation based upon a $d_{x^2-y^2}$ gap (Bulut et al. [75]), which is described in Section 3.

Fig. 4. The inset shows $(\lambda(0)/\lambda(T))^2$ versus T for nominally pure $YBa_2Cu_3O_{6.95}$. The main figure shows the same data but plotted as $(\lambda(0)/\lambda(T))^3$ versus T. The value of $\lambda(0)$ was taken to be 1400 Å (from [18]).

based upon the antiferromagnetic nature of the undoped system which involve $d_{x^2-y^2}$ pairing or possible $s + id_{x^2-y^2}$ pairing (see Appendix A), or alternatively, strongly correlated semion gauge models with $d_{x^2-y^2} + id_{xy}$ pairing [11,12]. There has also been the suggestion that the driving term responsible for pairing is the interlayer hopping [13] which is predicted to give rise to anisotropic s-wave pairing [14]. Finally, various triplet pairing schemes have also been discussed, [15] but as shown in Fig. 3, Knight shift [16,17] data imply that the pairs are singlet. In addition, recent measurements of the penetration depth, [18] plotted in Fig. 4, show that near T_c the superfluid density varies as

$$n_s = \left(\frac{\lambda(0)}{\lambda(T)}\right)^2 \sim \left(1 - \frac{T}{T_c}\right)^{\nu}, \tag{1}$$

with an index $\nu = 0.66$, which is consistent with three-dimensional XY universality[1]. Thus it would appear that we should be looking for singlet pairing in a one-dimensional representation.

In classifying the possible symmetry representations for the gap, we will frame the discussion in terms of the idealized case of a tetragonal lattice. As is known, the cuprate superconductors have a slight orthorhombic distortion, and, following the discussion of the tetragonal lattice, we will comment on the orthorhombic case. The five even parity irreducible representations [20,21] for a tetragonal lattice with D_{4h} symmetry are listed in Table 1, along with some representative basis gap functions. Four of these representations are one-dimensional. Some of the basis functions correspond to gap

[1] The possibility of observing critical behavior for the high-temperature superconductors is associated with their relatively short low-temperature coherence length. The fact that 3D behavior is observed near T_c is due to the divergence of $\xi_\perp$ linking the planes as T_c is approached. Specific heat measurements suggesting critical scaling consistent with 3DXY universality have been reported by G. Mozurkewich et al. [19].

Table 1
Even parity irreducible representations of D_{4h} along with examples of basis functions for Δ_k.

Irreducible representation	Basis functions for Δ_k
Γ_1^+	$1, \quad \cos k_x + \cos k_y$
Γ_2^+	$\sin k_x \sin k_y (\cos k_x - \cos k_y)$
Γ_3^+	$(\cos k_x - \cos k_y)$
Γ_4^+	$\sin k_x \sin k_y$
Γ_5^+	$\sin k_x \sin k_z, \quad \sin k_y \sin k_z$

functions which have been discussed as potential candidates for the high-T_c cuprates. The extended s-wave

$$\Delta_{s^*}(k) = \Delta_0(\cos k_x + \cos k_y), \tag{2}$$

is a basis state of Γ_1^+, and the d-waves

$$\Delta_{d_{x^2-y^2}}(k) = \Delta_0(\cos k_x - \cos k_y) \tag{3}$$

and

$$\Delta_{d_{xy}}(k) = \Delta_0 \sin k_x \sin k_y \tag{4}$$

are from Γ_3^+ and Γ_4^+, respectively. Figs. 5(a)–(c) give schematic plots of several different gap functions $\Delta(k)$ shown as solid lines relative to the shaded Fermi surface of a doped near-neighbor tight-binding band.

On a simple square lattice, the pair fields corresponding to the gap functions, Eqs. (2)–(4), are made up from different linear combinations of local singlet pairs. For example, the $d_{x^2-y^2}$-wave pair field operator

$$\tilde{\Delta}^\dagger_{d_{x^2-y^2}} = \sum_k \Delta_{d_{x^2-y^2}}(k) c^\dagger_{k\uparrow} c^\dagger_{-k\downarrow}, \tag{5}$$

with $c^\dagger_{ks}$ the creation operator for an electron of momentum k and spin s, can be expanded in terms of the site operators $c^\dagger_{ls}$ to give

$$\begin{aligned}\tilde{\Delta}^\dagger_{d_{x^2-y^2}} = \frac{\Delta_0}{2} \sum_l [&(c^\dagger_{l+x\uparrow} c^\dagger_{l\downarrow} - c^\dagger_{l+x\downarrow} c^\dagger_{l\uparrow}) - (c^\dagger_{l+y\uparrow} c^\dagger_{l\downarrow} - c^\dagger_{l+y\downarrow} c^\dagger_{l\uparrow}) \\ &+ (c^\dagger_{l-x\uparrow} c^\dagger_{l\downarrow} - c^\dagger_{l-x\downarrow} c^\dagger_{l\uparrow}) - (c^\dagger_{l-y\uparrow} c^\dagger_{l\downarrow} - c^\dagger_{l-y\downarrow} c^\dagger_{l\uparrow})].\end{aligned} \tag{6}$$

The lattice coordinate representation on the right corresponds to a $d_{x^2-y^2}$ linear combination of singlets between the l^{th} lattice site and its four near neighbors.[2]

Now in fact the point group of the cuprates, in the temperature and doping regime of interest, is orthorhombic D_{2h}. In this lower symmetry structure, the reflections $x = \pm y$ and the 90° rotation about the z-axis are removed, leaving the $d_{x^2-y^2}$ gap invariant under the allowed symmetry operations of D_{2h}. Thus in D_{2h}, the $d_{x^2-y^2}$ gap also belongs to the Γ_1^+ representation, and on purely symmetry

[2] In Appendix B we provide some further background regarding what is meant by "$d_{x^2-y^2}$ pairing."

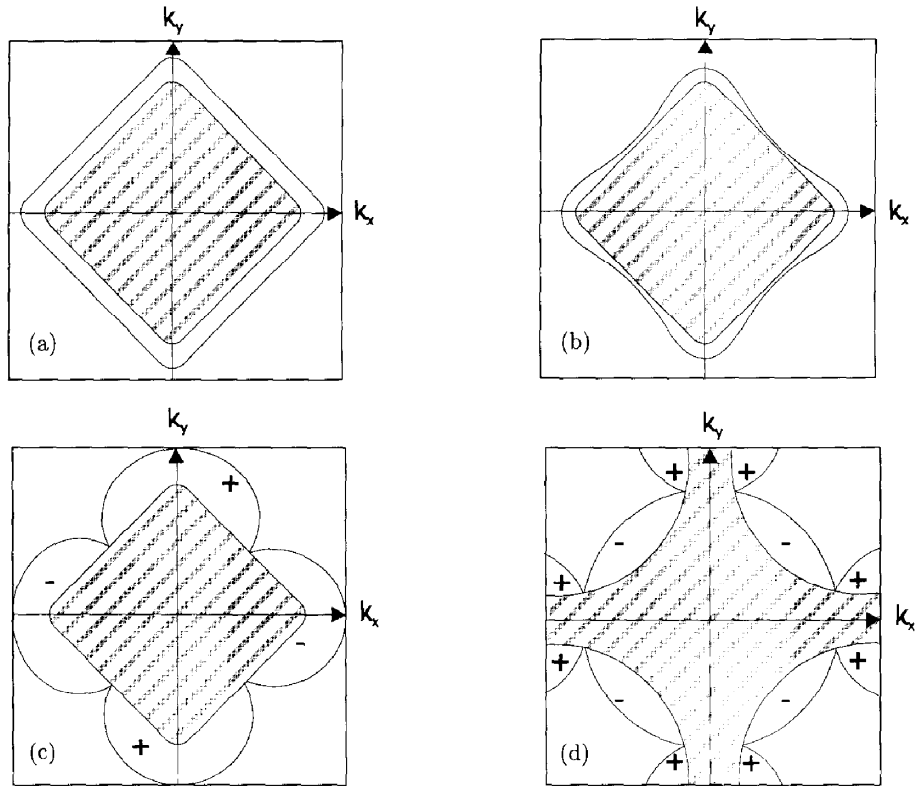

Fig. 5. Schematic plots of (a) an extended s-wave gap, (b) an anisotropic s-wave gap, (c) a $d_{x^2-y^2}$ gap, and (d) an extended s^*-wave gap for a Fermi surface of a system with a second near-neighbor hopping t'. The boundary of the shaded region is the normal state Fermi surface and the size of the gap Δ_k at the momentum k on the Fermi surface is indicated by the solid curve surrounding the Fermi surface. The gap in (a) and (b) has the same phase for all k, while the $d_{x^2-y^2}$ gap shown in (c) and the extended s^*-wave gap shown for the t' altered Fermi surface in (d) change sign as indicated.

grounds no distinction can be made between it and the extended or generalized s^*-wave. A Γ_1^+ gap would in general contain a mixture of the allowed basis functions, although for a nearly tetragonal system one would expect the combinations to be dominantly s^*- or $d_{x^2-y^2}$-like. Thus the following discussion is based upon the tetragonal classification, and, furthermore, we will often simply use one of the basis states given above and shown in Fig. 5 to characterize the gap. As shown in Fig. 5(d), one final caution to keep in mind is that when a second-nearest-neighbor hopping t' is included, a generalized s-wave gap can have eight (or a multiple of eight) nodes on the Fermi surface [21], so one must be careful about drawing conclusions regarding the symmetry of the gap based simply upon the presence of nodes.

2. Why might it happen?

In addressing the first question regarding why $d_{x^2-y^2}$ pairing might occur, we will look for the pairing mechanism in a model of a single CuO_2 layer and neglect the interlayer hopping. Our view is

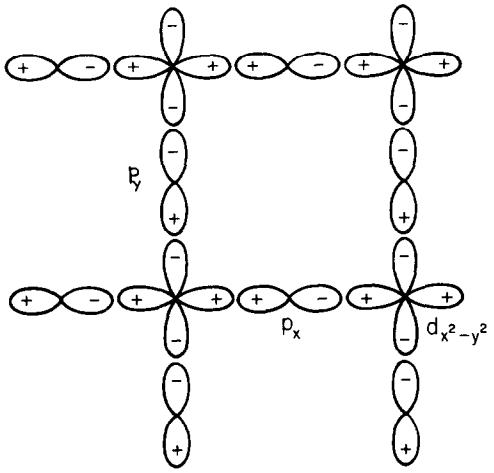

Fig. 6. Schematic of the CuO_2 plane and the one-electron $d_{x^2-y^2}$ Cu orbitals and the p_σ O orbitals that give rise to the band in which the pairs form.

that the interlayer hopping provides a weak coupling between the layers leading to a three-dimensional superconducting state but that the basic pairing mechanism resides in the CuO_2 plane. Fig. 6 contains a schematic of a CuO_2 plane and the one-electron $d_{x^2-y^2}$ Cu orbitals and p_σ O orbitals which have been used as the basis for various three-band extended Hubbard models [22] of the CuO_2 layer. An additional "folding-down" of this basis [23–26] leads to the one-band Hubbard model [27] which we will discuss. In this case, the system is simplified to nominal "Cu-sites" connected by an effective one-electron transfer t and having an onsite repulsion U which acts if two electrons occupy the same site,

$$H = -\sum_{\langle ij\rangle s} t(c_{is}^\dagger c_{js} + c_{js}^\dagger c_{is}) + \sum_i U n_{i\uparrow} n_{i\downarrow}. \tag{7}$$

Here $c_{is}^\dagger$ creates an electron of spin s on site i and n_{is} is the number operator $c_{is}^\dagger c_{is}$. There are, in principle, next-near-neighbor one-electron hopping terms which provide a more realistic model of the band structure and Fermi surface, but we will neglect them for our present discussion and take the $\langle ij\rangle$ sum in Eq. (7) over near neighbors. It is important to also recognize that in going from the three-band model for the CuO_2 sheet shown in Fig. 6 to the one-band model described by Eq. (7), we are ignoring the fact that the cuprates are charge transfer insulators [8] as well as the possibility that charge-transfer fluctuations may provide a pairing mechanism [10]. In defense of the one-band Hubbard model, Monte Carlo simulations of the three-band Hubbard model [28,29] near a band filling of one hole exhibit many of the same features as those found in sumulations of the one-band case near half-filling.

Within the Hubbard model framework there have been a variety of calculations which suggest that when the system is doped slightly away from half-filling, the on-site Coulomb interaction can give rise to superconductivity. These studies have varied from weak-coupling perturbation theory to strong-coupling variational calculations. They include exact diagonalization studies of small clusters and Monte Carlo simulations of larger clusters. They range from conserving approximations to phenomenological treatments. What is remarkable is the almost universal conclusion that if the two-

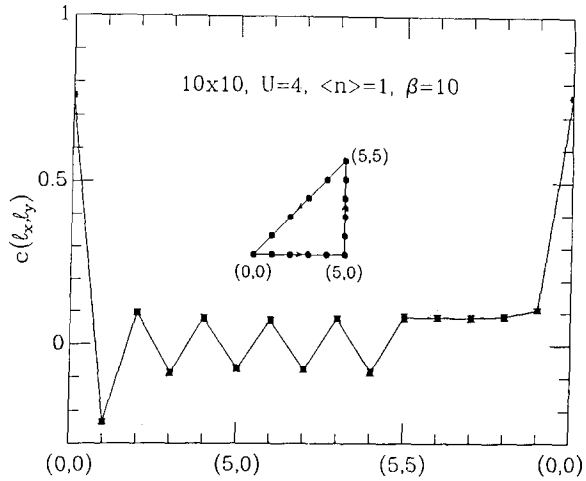

Fig. 7. Monte Carlo results for the spin-spin correlation function $c(l) = \langle m^z_{i+l} m^z_i \rangle$ versus position, with l moving along the path shown in the inset, for a 10×10 lattice at half-filling $\langle n \rangle = 1$. Here $U = 4t$ and the temperature $T = 0.1t$.

dimensional Hubbard model (or various t–J as well as related phenomenological models based upon the interaction of quasi-particles with antiferromagnetic spin-fluctuations) becomes superconducting when it is doped near half-filling, it will go into a $d_{x^2-y^2}$ state. In Appendix A we give a short summary of the various approaches [30]. Here we proceed with a discussion based upon intuition developed from Monte Carlo simulations and diagrammatic calculations.

In the half-filled state in which $\langle n_{i\uparrow} + n_{i\downarrow} \rangle = 1$, quantum Monte Carlo simulations show that the ground state of Eq. (7) has antiferromagnetic long-range order [31,32]. Physically, at half-filling when U is large, each site typically has one electron. If the spins on neighboring sites are oppositely oriented, then they can virtually hop over and back, lowering the energy of the system by a term proportional to $-t^2/U$. This is the strong-coupling result for the exchange interaction $J = 4\,t^2/U$ that gives rise to the antiferromagnetic correlations illustrated in Fig. 7. Here Monte Carlo results [32] for the spin-spin correlation function

$$c(l) = \langle m^z_{i+l} m^z_i \rangle, \tag{8}$$

with $m^z_i = n_{i\uparrow} - n_{i\downarrow}$, are shown for a 10×10 periodic lattice at a temperature $T = 0.1\,t$ with $U/t = 4$. At this temperature, the antiferromagnetic correlation length is larger than the lattice dimension used in this simulation. Finite-size scaling calculations using this type of Monte Carlo data have shown that the $\langle n \rangle = 1$ ground state has long-range antiferromagnetic order [31,32].

When the system is doped with holes so that, for example, $\langle n \rangle = 0.87$, the long-range antiferromagnetic order disappears, but the wave vector dependent magnetic susceptibility remains peaked at large momentum transfers. In Fig. 8, we show Monte Carlo results for the wave vector dependent susceptibility [32]

$$\chi(q) = \frac{1}{N} \sum_l \int_0^\beta d\tau \, \langle m^z_{i+l}(\tau) m^z_i(0) \rangle \, e^{iq \cdot l} \tag{9}$$

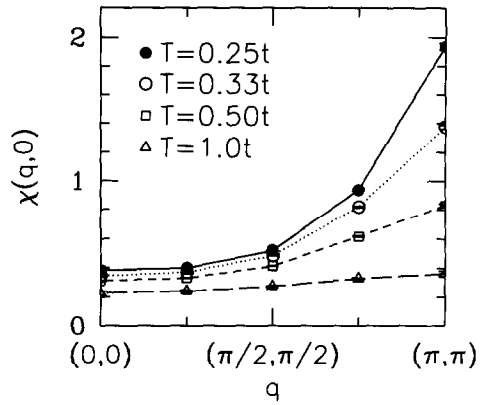

Fig. 8. Monte Carlo results for $\chi(q)$ versus q along the (1, 1) axis for various temperatures. Here $U = 4t$ and the filling $\langle n \rangle = 0.87$.

at various temperatures. As the system is cooled, we see that $\chi(q)$ develops short-range antiferromagnetic correlations. At still lower temperatures, on larger lattices the peak at (π, π) splits, [33] giving rise to incommensurate peaks at $(\pi - \delta, \pi)$ and $(\pi, \pi - \delta)$.

It turns out that for intermediate coupling, the simple RPA form

$$\chi(q) = \frac{\chi_0(q)}{1 - \bar{U}\chi_0(q)}, \tag{10}$$

with a parameterized (reduced) interaction $\bar{U}$, provides a useful approximation for χ [34,35]. Here

$$\chi_0(q) = \frac{1}{N}\sum_p \frac{f(\varepsilon_{p+q}) - f(\varepsilon_p)}{\omega - (\varepsilon_{p+q} - \varepsilon_p) + i\delta}, \tag{11}$$

with $\varepsilon_p = -2t(\cos p_x + \cos p_y) - \mu$ and f the usual Fermi function. The RPA diagrams for the longitudinal χ_{zz} and transverse χ_{+-} susceptibilities are shown in Fig. 9(a).

Near half-filling the nearly antiferromagnetic fluctuations which give rise to $\chi(q)$ are the dominant collective excitations, so that it is natural to examine the effective electron-electron interaction mediated by their exchange. Perturbation theory graphs for the exchange of longitudinal and transverse spin fluctuations are shown in Fig. 9(b). Comparing the graphs in Figs. 9(a) and 9(b) illustrates the nature of this process which gives rise to an effective electron-electron interaction introduced by Berk and Schrieffer [36],

$$V_{\text{eff}} = \frac{U^2\chi_0(p' + p)}{1 - U\chi_0(p' + p)} + \frac{U^3\chi_0^2(p' - p)}{1 - U^2\chi_0^2(p' - p)}. \tag{12}$$

At large momentum transfer where $U\chi_0$ is near 1, Eq. (12) has the simple form (since p can go to $-p$ for an even parity gap)

$$V_{\text{eff}} \simeq \tfrac{3}{2}U^2\chi(p' - p), \tag{13}$$

with χ given by Eq. (10). Thus in this approximation V_{eff} has the same momentum dependence as χ shown in Fig. 8.

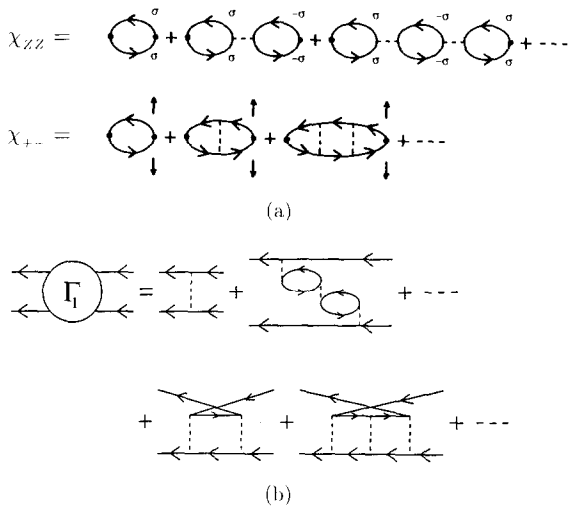

Fig. 9. (a) RPA diagrams for the longitudinal χ_{zz} and transverse χ_{+-} spin susceptibilities. (b) Diagrams for the effective interaction consisting of the exchange of longitudinal and transverse spin-fluctuations.

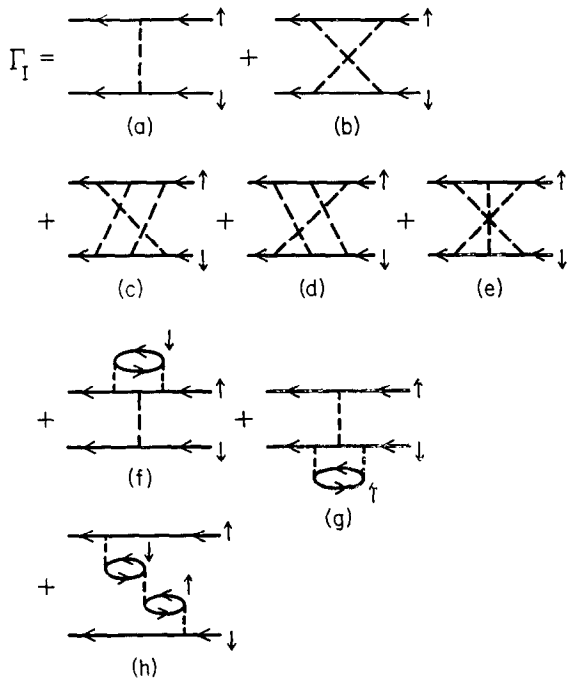

Fig. 10. The irreducible particle-particle interaction Γ_I and diagrammatic contributions through third-order.

More generally, we would like to know the momentum and energy (Matsubara frequency) dependence of the irreducible particle-particle interaction Γ_I shown in Fig. 10. Diagrams for Γ_I, through third-order are also shown in Fig. 10. The RPA approximation, Eq. (12), includes the contributions from Figs. 10(a), (b), (e), and (h) and sums the set of graphs shown in Fig. 9(b) to all orders.

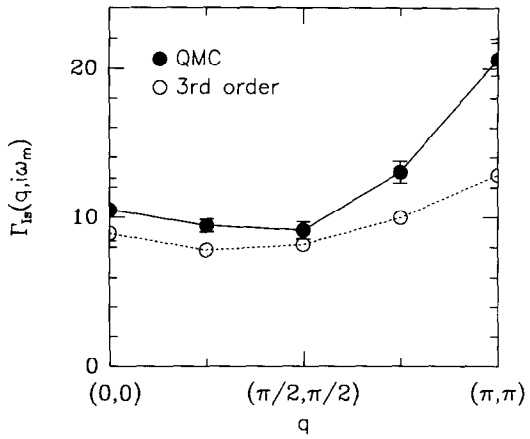

Fig. 11. The irreducible singlet particle-particle interaction $\Gamma_{1s}(q, \omega_m = 0)$ versus q along the (1, 1) direction for $\langle n \rangle = 0.87$, $U = 4t$, and $T = 0.25t$. The solid points are Monte Carlo data and the open circles are third-order perturbation theory results.

However, in the absence of a small parameter, the cross-graphs (c) and (d) as well as the vertex corrections (f) and (g) may not be negligible, and Eq. (12) is an uncontrolled approximation. Now, it is possible to use Monte Carlo simulations to calculate the complete irreducible particle-particle interaction Γ_1, and this has been done [37] on an 8×8 lattice with $U/t = 4$, $\langle n \rangle = 0.875$, at a temperature $T = 0.25t$. The results, which were obtained for the singlet channel with $\boldsymbol{q}$ along the $q_x = q_y$ axis, are plotted in Fig. 11 as the solid points. The open circles represent the third-order perturbation theory calculation for comparison. Just as found from the RPA interaction, the irreducible particle-particle interaction in the singlet channel, Γ_{1s} increases at large momentum transfers. Note that while the bare interaction $U = 4t$, Γ_{1s} becomes greater than $20t$ for $q = (\pi, \pi)$, even at the relatively high temperature $T = 0.25t$, at which this simulation was run.

Now, at this stage, let us pause in order to understand the nature of the attractive interaction represented by Γ_{1s}. The effective interaction plotted in Fig. 11 is positive. Can such an interaction cause pairing? The answer is yes, but to get a physical feeling for how this occurs, it is useful to look at the interaction in real space,

$$\Gamma_{1s}(\boldsymbol{l}) = \frac{1}{N} \sum e^{i\boldsymbol{q}\cdot\boldsymbol{l}} \Gamma_{1s}(q). \tag{14}$$

The real space Fourier transform of the Monte Carlo results for Γ_{1s} are plotted in Fig. 12. Here one sees that if two electrons are on the same site, $\Gamma_{1s}(l)$ is large and repulsive. However, if they are on near-neighbor sites, $\Gamma_{1s}(l)$ is attractive. Viewed in this way, the interaction appears as a giant Friedel oscillation, and if the two electrons can spatially arrange themselves to take advantage of the attractive regions of the interaction, it is possible that they can pair. In fact, Monte Carlo calculations of the Bethe-Salpeter equations [38] show that the interaction Γ_{1s} is attractive in the $d_{x^2-y^2}$ pairing channel. To understand this, consider the BCS gap equation

$$\Delta_p = -\sum_{p'} V_{pp'} \frac{\Delta_{p'}}{2E_{p'}}, \tag{15}$$

with p and p' near the Fermi surface shown in Fig. 5(b). If $V_{pp'} = \Gamma_{1s}(p' - p)$ is positive with its

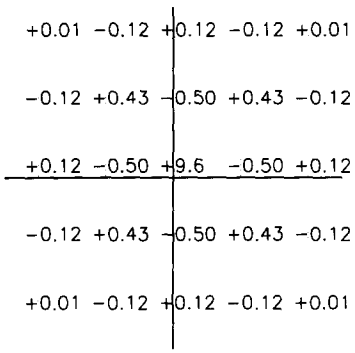

Fig. 12. Real space Fourier transform of the irreducible singlet vertex $\Gamma_{1s}(l, \omega_m = 0)$ versus the separation l between the pairs.

greatest strength at large momentum transfer, then from Eq. (15) it follows that Δ_p must change sign on the Fermi surface as illustrated in Fig. 5(c). Self-consistent conserving calculations [39,40] based on the spin-fluctuation exchange diagrams which include the full momentum and Matsubara frequency dependence give a low-temperature gap in close agreement with the simple $d_{x^2-y^2}$ form $\Delta_0(\cos p_x - \cos p_y)$.

It is interesting to contrast this interaction with the effective interaction for a weak-coupling low-temperature superconductor. In this case,

$$V_{\text{eff}} = \frac{-2|g_q|^2\omega_q}{\omega_m^2 + \omega_q^2} + \frac{4\pi e^2}{q^2 + \kappa_s^2}, \tag{16}$$

with the first term arising from the phonon exchange and the second term the screened Coulomb interaction. Even when the polarization sum and Umklapp processes are included, the screened Coulomb term severely reduces V_{eff} and can even make it positive. However, if we examine the interaction Eq. (16) in time, we find that

$$\begin{aligned} \text{Re}\,\langle V_{\text{eff}}(t)\rangle &= \text{Re}\int \frac{d\omega}{2\pi}\, e^{-i\omega t}\,\langle V_{\text{eff}}(i\omega_m \to \omega + i\delta)\rangle \\ &= -\langle |g_q|^2 \sin\omega_q t\rangle + \left\langle \frac{4\pi e^2}{q^2 + \kappa_s^2}\right\rangle \delta(t). \end{aligned} \tag{17}$$

Here the brackets denote an average of the momentum transfer q over the Fermi surface. The point is that the Coulomb interaction acts only over a short time, here represented by a broadened δ-function and set by the inverse bandwidth (or the plasma frequency, if it is smaller than the bandwidth), while the attractive electron-phonon interaction is retarded by the slower lattice response. Thus if the electrons making up the pair correlate themselves in time to avoid the short-time Coulomb repulsion, they can then take advantage of the attractive electron-phonon mediated interaction. This behavior is seen in the frequency dependence of the gap found by solving the Eliashberg equations [41]. $\text{Re}\Delta(\omega)$ increases as the typical phonon energy ω_0 is approached, goes negative when ω exceeds ω_0 and the lattice response is out of phase with the drive, and then *remains negative* out to large values of ω. This latter feature simply reflects the fact that the electrons making up the pair avoid short-time close-range encounters. It means that

$$\int_{\Delta}^{\infty} d\omega \left\langle \frac{4\pi e^2}{q^2 + \kappa_s^2} \right\rangle \frac{\Delta(\omega)}{\omega} \simeq 0, \tag{18}$$

or that in practice $\langle 4\pi e^2/(q^2 + \kappa_s^2)\rangle$ can be replaced over the frequency interval Δ to several times the Debye energy by a weak pseudo-potential [42]. Now an analogous thing happens for $d_{x^2-y^2}$ pairing in the Hubbard model. That is, the two pairing electrons avoid the Coulomb interaction by arranging themselves in space in a $d_{x^2-y^2}$ orbit. In this case the gap changes sign in momentum space, $\Delta_p = \Delta_0(\cos p_x - \cos p_y)$, and

$$\sum_p \frac{U\Delta_p}{2E_p} = 0. \tag{19}$$

This same effect is clearly seen in Fig. 12 where the repulsive interactions associated with the 45° and 135° lattice sites are avoided by the nodes of a $d_{x^2-y^2}$ gap.

These ideas have basically been weak coupling arguments. There are also a variety of strong coupling pictures which have been developed. These often start from the t–J model (formally, the large U limit of the Hubbard model) discussed in Appendix A. In this model, there is a Heisenberg antiferromagnetic coupling J between spins on adjacent sites and holes move via a hopping t. A generalization beyond the Hubbard model treats t and J as independent parameters. Perhaps the simplest strong coupling pairing picture to visualize is the notion that two holes will seek to occupy adjacent sites in order to break seven exchange bonds rather than eight. Unfortunately, this is too classical a view, and by the time it can occur, one is likely to be in the phase separation [43] region of the t–J model. Exact diagonalization calculations, which indicate that a $d_{x^2-y^2}$ bound state of two holes can form, [44] find that the two bound holes are typically separated by more than one site at weaker (physical) values of J/t. Here the physical picture may be closer to the kinetic energy based idea that two correlated holes can move more freely through the locally antiferromagnetic lattice with one unzipping the ferromagnetic string created by the motion of the other. It appears that there is a continuous crossover between the weak-coupling and strong-coupling pictures and that both favor $d_{x^2-y^2}$ pairing.

Given this, an important question remains: is the Coulomb induced quasi-particle spin-fluctuation interaction the dominant coupling in the cuprates relative to the electron-phonon and charge-transfer fluctuation interactions? One answer to this is given by transport calculations which show that the size and over-all temperature dependence of the normal state resistivity can be adequately described by a spin-fluctuation exchange model [45,46]. Of particular interest is the fact that these same models also provide an explanation of the NMR (NQR) relaxation rates [47–51]. Further support for this is provided by experiments on YBCO which clearly show that changes in the spin-fluctuation spectrum observed in NMR experiments are accompanied by changes in the normal state resistivity and the Hall coefficient. The in-plane resistivity $\rho_{ab}(T)$ and the Hall coefficient $R_H(T)$ of $YBa_2Cu_3O_{7-y}$ have been measured for various oxygen concentrations [52]. In the oxygen-depleted materials, $\rho_{ab}(T)$ deviates from a linear T dependence and $R_H(T)$ deviates from T^{-1} below a temperature T^*. This deviation was found to coincide with the opening of a spin gap at T^* as seen in NMR [17] and neutron scattering experiments [53]. Similar behavior was observed in the two-chain $YBa_2Cu_4O_8$ compound [54,55], which is stoichiometric and untwinned with the chains running along the b-axis. For $YBa_2Cu_4O_8$, the resistivity measured along the a-axis probes the charge transport associated

with the CuO_2 planes. Just as for the $YBa_2Cu_3O_{7-y}$, the temperature deviates from the linear T dependence below a $T^* \sim 200$ K, where from NMR measurements of Zimmermann et al. [56] there is evidence for the opening of a spin gap. There is a clear correlation between ρ_a/T, the Cu(2) Knight shift, and $(T_1T)^{-1}$ versus T. A plausible explanation for the correlation between these quantities in both $YBa_2Cu_3O_{7-y}$ and $YBa_2Cu_4O_8$ is that the transport in the normal state of the CuO_2 planes is dominated by spin-fluctuation scattering and that the opening of a spin gap leads to a reduction in this scattering [55]. In addition, the rapid drop in the quasi-particle inelastic scattering rate for $T < T_c$ observed in $YBa_2Cu_3O_{6.95}$ by Bonn et al. [57] is similar to the decrease in the nuclear relaxation rate. Calculations of the quasi-particle lifetime due to spin-fluctuation scattering [58] leads to results in good agreement with the experimental observations.

So to summarize the discussion of why $d_{x^2-y^2}$ pairing might occur:

- 1. The observed correlation of resistivity, optical and microwave conductivity data with NMR and neutron scattering results are consistent with the notion that the dominant quasi-particle scattering mechanism in the cuprates involves spin-fluctuations. The Hubbard model as well as the t–J model provides a description of these spin-fluctuation processes.
- 2. Diagrammatic as well as Monte Carlo calculations for the Hubbard model find that near half-filling, spin-fluctuation exchange leads to an effective electron-electron interaction which is attractive in the singlet $d_{x^2-y^2}$ channel. The $d_{x^2-y^2}$-wave pairs avoid the on-site Coulomb repulsion. In addition, a variety of different numerical, diagrammatic, and phenomenological calculations reviewed in Appendix A find that for the t–J model as well as the Hubbard model, there is an attractive interaction in the singlet $d_{x^2-y^2}$ channel.

Having said this, it is important to keep in mind Feynman's warning, [59] "The first principle is that you must not fool yourself—and you are the easiest person to fool." There are a number of questions which can be raised regarding the $d_{x^2-y^2}$-wave scenario we have discussed.

- 1. Is the Hubbard model really the right starting point? Neutron scattering experiments on YBa_2Cu-$O_{7-\delta}$ with δ near zero (optimal doping) have so far failed to exhibit strong antiferromagnetic fluctuations [60]. Perhaps the correlation between changes in the transport properties and the magnetic properties simply reflect a common underlying feature associated with a quite different mechanism involving, for example, charge-transfer [10] or incipient-phase separation [43]. Are we being fooled by our apparent ability to fit some of the transport data using spin-fluctuation approximations?
- 2. The diagrammatic calculations only sum selected graphs and there is no small parameter. Monte Carlo simulations of the Hubbard model have failed to find evidence for the spatial growth of pair-field correlations [61,62] or evidence for a finite superfluid density at the temperatures and lattice sizes that have been studied [63,64]. Furthermore, the zero-temperature exact diagonalization calculations for the Hubbard model have only been carried out on small (4×4) lattices [65]. While extrapolated results have been obtained for two holes in a t–J model, these calculations neglect the three-site t^2/U terms, and it is not known what happens on large lattices at a fixed density of holes [66].

Thus it is of great interest to understand how we would know from experiment whether the gap has $d_{x^2-y^2}$ symmetry. While the existence of a $d_{x^2-y^2}$ gap would not uniquely imply that the antiferromagnetic spin-fluctuation mechanism is responsible for pairing in the cuprates, it would certainly be consistent with what is expected from such an interaction. Furthermore, if the gap is not close to the $d_{x^2-y^2}$ form it would provide a strong incentive to look for alternative pairing mechanisms.

3. How would we know?

Shortly after the discovery of the high-T_c cuprates, Shapiro steps [67] at voltage increments $hf/2e$ were seen in weak links irradiated by microwaves of frequency f, and flux quantization in units of $hc/2e$ was observed in flux lattice studies [68] showing that the superconducting order parameter involved pairs of electrons. Furthermore, Knight shift measurements [16,17], Fig. 3, below T_c provided evidence that the electron pairs were in a singlet state, and the critical behavior [18] of n_s, Fig. 4, implies that we are looking for a non-degenerate orbital state[3]. Thus, as discussed in the introduction, the remaining question involves the symmetry of the orbital state.

Quasi-particle properties. The low-temperature dependence of various thermodynamic and transport properties depends upon the quasi-particle density of states $N(\omega)$. If the gap has nodes (line nodes in 3D), then $N(\omega)$ at low energies for the pure system varies linearly with ω and the low-temperature quasi-particle properties vary as power laws. Alternatively, if the magnitude of the gap does not vanish, the low-temperature density of quasi-particles and their contribution to transport properties decreases exponentially. Here we review some examples of quasi-particle properties which show power-law behavior consistent with a $d_{x^2-y^2}$ gap. In addition, we will examine how impurities alter this behavior.

In the usual BCS theory, the penetration depth is given by

$$\left(\frac{\lambda(0)}{\lambda(T)}\right)^2 = 1 - 2\beta \int_0^\infty d\omega \frac{N(\omega)}{N_0} f(\omega)(1 - f(\omega)), \tag{20}$$

with $N(\omega)$ the quasi-particle density of states normalized to the normal state single-spin density of states N_0. Here, for a constant s-wave gap,

$$N(\omega)/N_0 = Re[\omega/(\omega^2 - \Delta_0^2)^{1/2}], \tag{21}$$

while for a gap with a node, such as a $d_{x^2-y^2}$ gap, at an energy ω which is small compared to the maximum (anti-node) value of the gap Δ_0,

$$\frac{N(\omega)}{N_0} \cong \frac{\omega}{\Delta_0}. \tag{22}$$

For an s-wave gap, the number of quasi-particles is exponentially small at low temperatures, and Eq. (20) gives the well known s-wave BCS result

$$\frac{\lambda(T) - \lambda(0)}{\lambda(0)} \cong \left(\frac{2\pi\Delta}{T}\right)^{1/2} e^{-\Delta/T}. \tag{23}$$

However, for a clean $d_{x^2-y^2}$ material with a density of states given by Eq. (22), one finds from Eq. (20) that

[3] In particular, the smooth temperature dependence of $\lambda(T)$ is supportive of a single phase transition, ruling out scenarios in which the system initially condenses into a $d_{x^2-y^2}$ phase and subsequently makes a second phase transition into a $d_{x^2-y^2} + is$ or $d_{x^2-y^2} + id_{xy}$ phase.

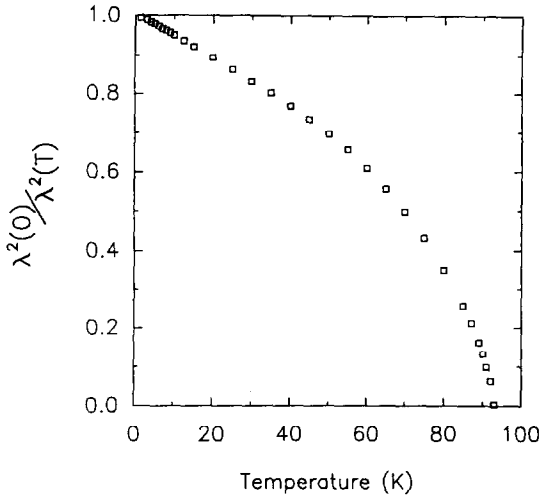

Fig. 13. Microwave data for $(\lambda(0)/\lambda(T))^2$ versus T for an $YBa_2Cu_3O_{6.95}$ crystal [69].

$$\frac{\lambda(T)-\lambda(0)}{\lambda(0)} \cong \ln(2)\frac{T}{\Delta_0}. \tag{24}$$

In Fig. 13, we show experimental measurements of the penetration depth by Hardy et al. [69] on a YBCO crystal. The low-temperature linear variation of $n_s/n = (\lambda(0)/\lambda(T))^2$ is clearly evident. For the pure crystal, the slope $4A/K$ of $\Delta\lambda(T)$ is close to $\lambda(0)\ln(2)/\Delta_0$.

As previously noted, for a clean system, a linear T dependence for $\lambda(T)$ might also arise if the gap is an extended or generalized s-wave with nodes (see Fig. 5(d)). Thus, to determine the symmetry of the gap, it is necessary to have a variety of probes. For example, high-resolution angular resolved photoemission can in principle distinguish between a $d_{x^2-y^2}$ gap and an extended s^*-wave gap of the type illustrated in Fig. 5(d).

Now it appears that the linear T dependence of $\lambda(T)$ is only seen in extremely pure systems. In fact, much of the early $\lambda(T)$ data failed to exhibit the linear T dependence and was in fact taken as providing evidence that the gap was nodeless. However, within the $d_{x^2-y^2}$ framework, it is now argued that the role of impurities is key. As discussed by Hirschfeld and Goldenfeld [70], a $d_{x^2-y^2}$ system with strong unitary impurity scattering develops a finite density of states $N(0)$ at zero energy and below a characteristic energy $T^* \sim (\Gamma\Delta_0)^{1/2}$ determined by the scattering rate $\Gamma = n_i/\pi N(0)$, with n_i the impurity concentration

$$N(\omega) \cong N(0) + a\omega^2, \tag{25}$$

with $N(0) \sim (\Gamma/\Delta_0)^{1/2}N_0$. Above this energy $N(\omega) \cong (\omega/\Delta_0)N_0$. In this case

$$\lambda(T) = \lambda(0) + \Delta\lambda + \lambda(0)\ln(2)\frac{T^2}{T+T^*}, \tag{26}$$

with $\Delta\lambda = \frac{1}{2}(\Gamma/\Delta_0)^{1/2}\lambda(0)$. Thus a $d_{x^2-y^2}$ gap with strong scattering impurities gives a penetration depth $\lambda(T)$ which varies as T^2 below a crossover temperature T^* and then returns to a linear temperature variation for $T > T^*$ provided T^* is not so large that one moves out of the linear regime

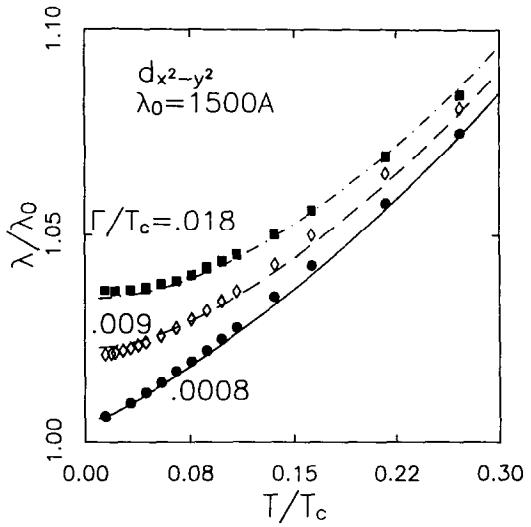

Fig. 14. Penetration depth $\lambda(T)$ versus T for Zn doped YBCO. Here $\lambda(T)$ is normalized to the zero temperature clean penetration depth λ_0. The theoretical curves [113] are calculated in the unitary scattering limit for the Γ/T_c ratios listed. The data [69] for the nominally pure YBCO crystal is shown as circles, for 0.15% Zn doping as diamonds and for 0.31% Zn doping as squares.

of the pure system. Fig. 14 shows the results of fitting $\lambda(T)$ to Eq. (26) for the Zn doped crystals of Hardy et al. [69] The shift $\Delta\lambda$ used in Fig. 14 is consistent with recent μsr measurements [71].

A similar analysis of the Knight shift and nuclear relaxation rate T_1^{-1} in Zn-doped $YBCO_7$ also provides a consistent interpretation of these measurements [72–74]. In particular, impurities lead to a zero temperature Knight shift proportional to $N(0) \sim (\Gamma/\Delta_0)^{1/2}N_0$, and as the temperature increases, K varies as T^2 until it crosses over to a linear T variation above T^*. At low temperatures, the longitudinal relaxation rate T_1^{-1} shows a low-temperature linear Korringa-like behavior with the effective density of states $N(0)$ and then crosses over to a T^3 variation discussed below.

To obtain a more complete description of the magnetic properties of the cuprates in the superconducting state, it is necessary to take into account the effect of the Coulomb correlations. Thus, for example, the spin-susceptibility has been described by an approximate RPA–BCS form [75]

$$\chi = \frac{\chi_0^{\mathrm{BCS}}}{1 - \overline{U}\chi_0^{\mathrm{BCS}}}. \tag{27}$$

This form was introduced as an approximate way of treating the effect of superconducting correlations on the strong antiferromagnetic Coulomb correlations. Here $\overline{U}$ is an effective interaction and χ_0^{BCS} is the BCS form for the magnetic susceptibility

$$\chi_0^{\mathrm{BCS}} = \frac{1}{N}\sum_p \left\{ \frac{1}{2}\left[1 + \frac{\varepsilon_{p+q}\varepsilon_p + \Delta_{p+q}\Delta_p}{E_{p+q}E_p}\right] \frac{f(E_{p+q}) - f(E_p)}{\omega - (E_{p+q} - E_p) + i\Gamma} \right.$$
$$\left. + \frac{1}{4}\left[1 - \frac{\varepsilon_{p+q}\varepsilon_p + \Delta_{p+q}\Delta_p}{E_{p+q}E_p}\right] \frac{1 - f(E_{p+q}) - f(E_p)}{\omega + (E_{p+q} + E_p) + i\Gamma} \right.$$

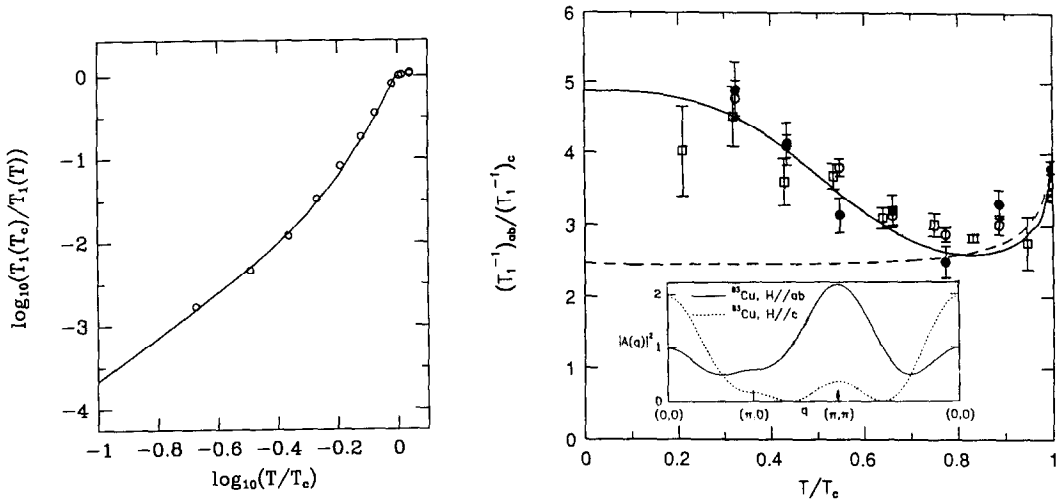

Fig. 15. (a) Temperature dependence of the nuclear relaxation rate of ^{63}Cu(2) with H along the c-axis normalized to its value at T_c versus T/T_c. Here a d-wave gap amplitude $2\Delta_0/kT_c = 8$ and a quasi-particle damping $\Gamma = T_c(T/T_c)^3$ have been assumed [75]. The experimental data are from Hammel et al. [77]. (b) Temperature dependence of the ^{63}Cu(2) anisotropy $(T_1^{-1})_{ab}/(T_1^{-1})_c$. The experimental data are from Martindale et al. [78] (squares) and Takigawa et al. [83] (filled and empty circles). The solid curve is for a $d_{x^2-y^2}$-wave gap and the dashed curve is for an s-wave gap (from [75]). The inset shows the q-dependence of the hyperfine form factor $|A(q)|^2$ versus q for H parallel to the ab plane (solid) and the c-axis (dashed).

$$+\frac{1}{4}\left[1+\frac{\varepsilon_{p+q}\varepsilon_p+\Delta_{p+q}\Delta_p}{E_{p+q}E_p}\right]\frac{f(E_{p+q})+f(E_p)-1}{\omega-(E_{p+q}+E_p)+i\Gamma}\Bigg\}, \tag{28}$$

with ε_p the band energy and Δ_p the gap. Eq. (28) contains the usual energy denominators and Fermi factors along with the well-known BCS coherence factors. The hyperfine Mila-Rice coupling constants [76], the band parameters and filling along with $\overline{U}$ can be taken from fits of the normal state NMR data. This leaves the form of the gap, the ratio $2\Delta(0)/kT_c$, and the quasi-particle lifetime as parameters which can be used to fit the NMR results for $T < T_c$. The Knight shift results shown as the dashed curve in Fig. 3 were obtained using Eqs. (27) and (28) with a $d_{x^2-y^2}$ gap. In Fig. 15(a) we compare experimental results [77] for the longitudinal spin-lattice relaxation rate of ^{63}Cu(2) with calculated values obtained from

$$\left(\frac{1}{T_1}\right)_c = \frac{T}{N}\sum_q |A_c(q)|^2 \left.\frac{\mathrm{Im}\,\chi(q,\omega)}{\omega}\right|_{\omega_z}, \tag{29}$$

with ω_z the Zeeman energy. Here $A(q)$ is the Mila-Rice hyperfine form factor for H parallel to the c-axis, $\chi(q,\omega)$ is given by Eqs. (27) and (28) with the simple Hubbard bandstructure $\varepsilon_p = -2t(\cos p_x + \cos p_y) - \mu$, and $\Delta_p = \Delta_0(T)(\cos p_x - \cos p_y)$. Note that the Hebel-Slichter peak is absent [78–80]. Within the $d_{x^2-y^2}$ picture, the absence of the Hebel-Slichter peak arises from a combination of effects [75]: (a) the d-wave single-particle density of states has only a logarithmic singularity at Δ_0 rather than the square-root singularity for an s-wave gap, (b) the coherence factor for quasi-particle scattering (the first term in Eq. (28)) vanishes for $q \sim (\pi,\pi)$ for a $d_{x^2-y^2}$ gap, and (c) the inelastic scattering acts to suppress the peak just as for an s-wave gap. At low temperatures,

the linear density of states arising from nodes in the $d_{x^2-y^2}$ gap imply tht T_1^{-1} varies as T^3. This is consistent with the observed behavior, see Fig. 15(a), but it will be interesting to have lower temperature data on clean materials to firmly establish the low-temperature T^3 behavior.

The $d_{x^2-y^2}$ form for Δ_k was also found to provide a possible explanation for the temperature dependence of the ^{63}Cu(2) anisotropy $(T_1^{-1})_{ab}/(T_1^{-1})_c$ associated with having H in the ab plane and along the c-axis, respectively [75]. The q-dependence of the hyperfine form factors for ^{63}Cu with the external magnetic field H in the ab plane or along the c-axis are quite different. This difference is reflected in the temperature dependence of the ratio $(T_1^{-1})_{ab}$ to $(T_1^{-1})_c$. As seen from the inset in Fig. 15(b), the form factor is such that the nuclear relaxation rate for ^{63}Cu when H is in the ab plane has a larger contribution from the (π, π) spin fluctuations than $(T_1^{-1})_c$ for H parallel to the c-axis. In the normal state $(T_1^{-1})_{ab}/(T_1^{-1})_c$ is found to increase with decreasing temperature due to the growth of antiferromagnetic fluctuations [81,82]. In the superconducting state, the observed anisotropy ratio $(T_1^{-1})_{ab}/(T_1^{-1})_c$ initially decreases as T drops below T_c but then increases at lower reduced temperatures [78,83–85] as shown in Fig. 15(b). The dashed curve shows the calculated anisotropy ratio obtained for an s-wave gap using Eqs. (27) and (28) in Eq. (29) along with the appropriate hyperfine form factors. While an s-wave gap gives the initial decrease of the anisotropy ratio associated with the opening of the gap, it is unable to account for the subsequent increase in the anisotropy ratio at lower reduced temperatures. The solid curve in Fig. 15(b) is the corresponding result for a $d_{x^2-y^2}$ gap [75]. Here again $(T_1^{-1})_{ab}/(T_1^{-1})_c$ initially decreases as the gap opens. However, at lower reduced temperatures the spin fluctuation spectral weight $\mathrm{Im}\,\chi(q, \omega)/\omega|_{\omega_z}$ decreases faster for small values of q than for large values of q near (π, π) due to the nodes in the $d_{x^2-y^2}$ gap. This causes the anisotropy ratio to increase, as shown in Fig. 15(b). It is important to note that in this calculation the parameter $\overline{U}$ in the RPA form for χ, Eq. (27), as well as the hyperfine form factors $A_{ab}(q)$ and $A_c(q)$ were kept the same as in the earlier work for the normal state. Only the form of the gap, $d_{x^2-y^2}$ or s-wave, the ratio $2\Delta(0)/kT_c = 8$ and the quasi-particle lifetime $\tau^{-1} \sim T_c(T/T_c)^3$ were chosen.

Thelen et al. [86] have extended this approach by including a next nearest neighbor hopping t' and a q dependent effective exchange $\overline{U}$ in Eq. (27). In this case, proper account of the YBCO Fermi surface is taken into account along with $\chi(q)$ and a quantitative fit to both the ^{63}Cu and ^{17}O NMR relaxation rates for $T < T_c$ are obtained. The interrelationship of the band structure and the spin dynamics in the cuprates has also been emphasized by Si et al. [51], and they have also carried out detailed calculations of the NMR relaxation times as well as the neutron-scattering response.

The transverse nuclear relaxation rate T_{2G}^{-1} was calculated using the same RPA–BCS form for χ. In this case, it is the real part of χ which enters and one has

$$\frac{1}{T_{2G}} \cong \left[\sum_q |A(q)|^4 \chi^2(q) - \left(\sum_q |A(q)|^2 \chi(q)\right)^2\right]^{1/2}. \tag{30}$$

In Fig. 16, the results of this calculation [87] are compared with measurements on $YBa_2Cu_4O_8$ by Itoh et al. [85]. The over-all scale of the theoretical calculation is set by the value chosen for the bandwidth. The calculation was done prior to the experiment and, as can be seen, the $d_{x^2-y^2}$-wave result is in good agreement with the measurement, although it is important to keep in mind that this is a technically difficult experiment because of the large r.f. field modulation required to sweep through the resonance line and avoid effects due to temperature-dependent changes in the linewidth. The large

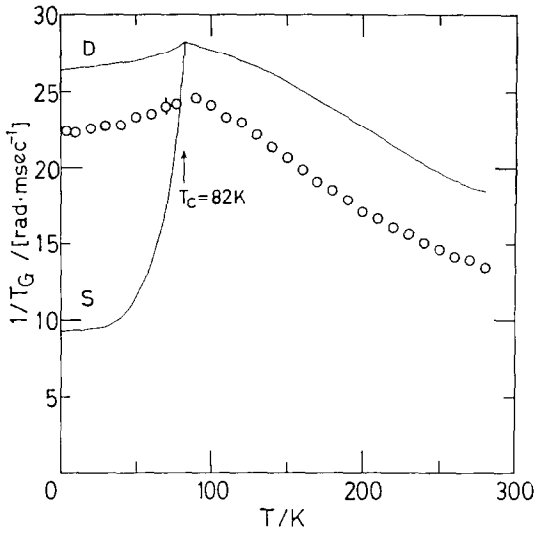

Fig. 16. The nuclear transverse relaxation rate for $^{63}Cu(2)$ versus temperature for $YB_2Cu_4O_8$ [72]. The curve D is the $d_{x^2-y^2}$-wave prediction and the curve labeled S is the s-wave predictions [87]. The over-all scale is set by the assumed value for the bandwidth.

decrease in T_{2G}^{-1} below T_c for an s-wave gap arises from the suppression of the antiferromagnetic correlations by the superconducting gap. For a $d_{x^2-y^2}$ gap, this suppression is significantly reduced due to the nodes and the existence of electronic states in the gap below Δ_0 where $N(\omega)$ varies as ω, Eq. (22).

There are in addition a variety of other transport measurements such as Raman scattering and inelastic neutron scattering which clearly show the existence of states in the gap. Devereaux et al. [88] have argued that the symmetry dependence of the Raman scattering in BSCCO implies that the gap has predominantly $d_{x^2-y^2}$ character. However, Krantz and Cardona [89] disagree with this interpretation of the data and furthermore stress the difficulty of using Raman spectroscopy to distinguish between a $d_{x^2-y^2}$ and a strongly anisotropic s-wave gap. Likewise, while the neutron scattering data of Mason et al. [90] clearly shows the presence of states in the gap, they note that the isotropic reduction of the peaks is inconsistent with the behavior of $\mathrm{Im}\,\chi_0^{BCS}(q,\omega)$ calculated from Eq. (28) with a $d_{x^2-y^2}$ gap. They propose that their data be interpreted in terms of a dirty s-wave gap. We [91] and others [92] have shown that when spin-fluctuation enhancement, Eq. (27), and impurity scattering are taken into account, a $d_{x^2-y^2}$ gap can provide a possible fit to the data. However, the absence of line width narrowing below T_c disagrees with present calculations unless a large amount of impurity scattering is included.

Angular resolved photoemission spectroscopy (ARPES) studies [93] provide information on the magnitude of the gap $|\Delta_k|$ on different parts of the Fermi surface. Fig. 17 shows measurements of Shen et al. [94] on a Bi 2212 crystal. There is a clear shift of spectral weight as the gap opens for a momentum k_A while the shift for k_B is negligible. These experiments probe the magnitude of the gap and hence cannot distinguish between a highly anisotropic s-wave and a $d_{x^2-y^2}$ gap. However, the experimentalists conclude that their results are consistent with a $d_{x^2-y^2}$ gap. It will be interesting to determine the effect of impurities on the ARPES. In such experiments it will be important to know

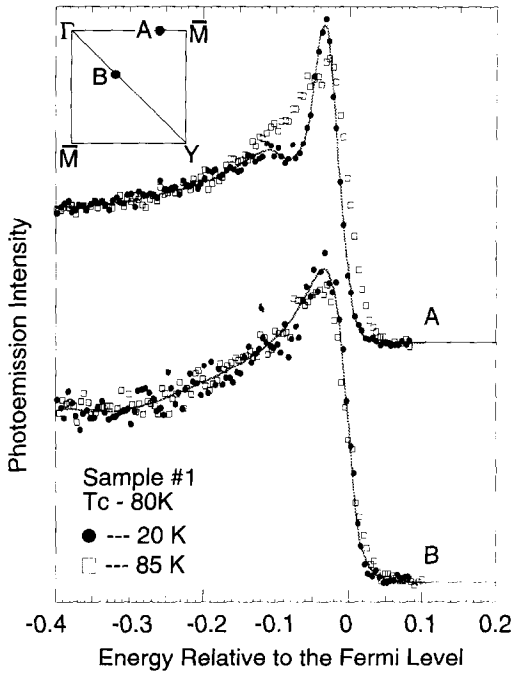

Fig. 17. ARPES data [94] above and below $T_c \simeq 79\,\mathrm{K}$ recorded at two Fermi surface wave vectors k_A and k_B marked in the inset. In the superconducting state the leading edge of the spectral weight shifts for k_A, indicating a gap. The absence of an observable shift at k_B implies a large gap anisotropy consistent with a $d_{x^2-y^2}$ gap.

that the impurities act on quasi-particles in the CuO_2 plane and not simply as surface contaminants which scatter the emitted electrons.

It is also possible to devise measurements which look at the relative phase of the gap between different points on the Fermi surface. Wollman et al. [95] have studied the magnetic flux modulation of dc SQUIDs in which YBCO–Au–Pb Josephson weak links fabricated on the orthogonal a and b faces of a YBCO single crystal are connected by a Pb film. These pioneering experiments are difficult because of SQUID asymmetries, the need to extrapolate to zero SQUID current, and the possibility of trapped flux. In addition Klemm [96] has pointed out the problem that a corner geometry presents with respect to flux penetration. Nevertheless, Wollman et al. [95] conclude that taken as a whole these experiments provide evidence for a π phase shift between pairs tunneling in the a and b directions. In addition, these authors have also reported results for the magnetic flux dependence of the critical current of a single Josephson junction formed on the corner of a YBCO crystal. In this case, for a junction whose dimensions are small compared to the Josephson penetration depth so that self-fields can be neglected, the critical-current-flux relation is

$$I_c(\Phi) = 2\,I_0 \sin^2(\pi\Phi/2\,\Phi_0)/(\pi\Phi/\Phi_0) \tag{31}$$

rather than the usual Fraunhofer form $I_c(\Phi) = 2I_0(\sin\pi\Phi/\Phi_0)/(\pi\Phi/\Phi_0)$. These ideal characteristics are shown as the solid (d-wave) and dashed (s-wave) curves in Fig. 18. Recent experimental results for a corner junction are shown in the lower part of Fig. 18. It would be useful to have a magnetic field scan to determine whether peculiar trapped flux configurations or inhomogeneous current flows

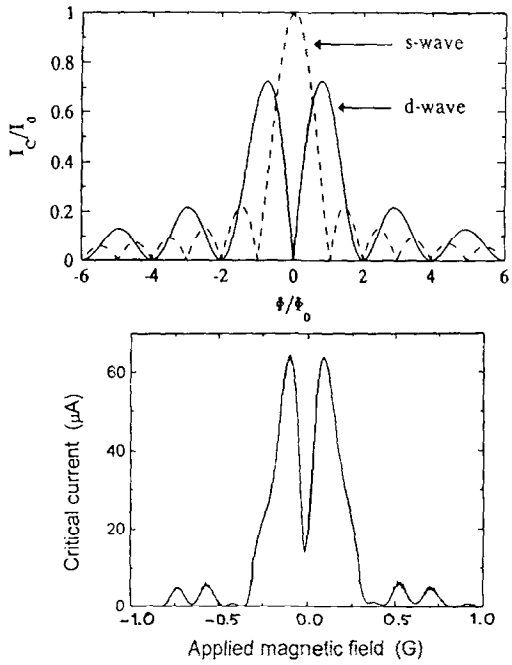

Fig. 18. The upper part of this figure shows the predicted current versus flux characteristics for a YBCO–Pb corner Josephson junction with YBCO assumed to have an s-wave (dashed) or a $d_{x^2-y^2}$-wave (solid) gap. The lower curve shows the experimental measurement of one such junction (from [95]).

are present. In addition, it would be interesting to compare these experiments with similar experiments on conventional low-temperature superconductors [97].

Recently Tsuei et al. [98] have reported studies of flux quantization in superconducting $YBa_2Cu_3O_{7-\delta}$ rings with 0-, 2-, and 3-grain boundary Josephson junctions. The geometry of the rings in this experiment is shown in Fig. 19. The rings studied in this work were fabricated from epitaxial films of YBCO deposited on a tri-crystal $SrTiO_3$ substrate. The YBCO film grows with its a–b axes oriented along the (100) and (010) axes of the $SrTiO_3$ substrate forming grain boundary Josephson junctions along the boundaries set by the tri-crystal geometry illustrated in Fig. 19. Then the rings are patterned such that one ring has no-grain boundaries, two rings have two-grain boundaries, and the ring in the center has three-grain boundaries. The orientations of the grain boundaries in the three-grain boundary junction are such that in the absence of any flux, one of the Josephson grain boundary junctions is frustrated, that is the phases associated with pair transport perpendicular to the interface have the opposite signs. We have schematically illustrated this in the figure. The point is that the Fermi surface is locked to the lattice, the phase of the pair field modulo an over-all phase factor $e^{i\varphi}$ is locked to the Fermi surface, and it is assumed that the pair field coupling across a grain boundary is mediated by electrons traveling perpendicularly to the interface. Now suppose the inductance of the ring L multiplied by the junction critical current I_c is large compared to a flux unit $hc/2e$. In this case, it requires very little magnetic energy to create half of a flux unit in the ring which can then provide a π phase shift to heal the frustrated grain boundary junction and recover the Josephson junction energy. Thus, as discussed by Sigrist and Rice [99], such a ring in the absence of an external field will have a spontaneous magnetization corresponding to half of the usual superconducting flux unit

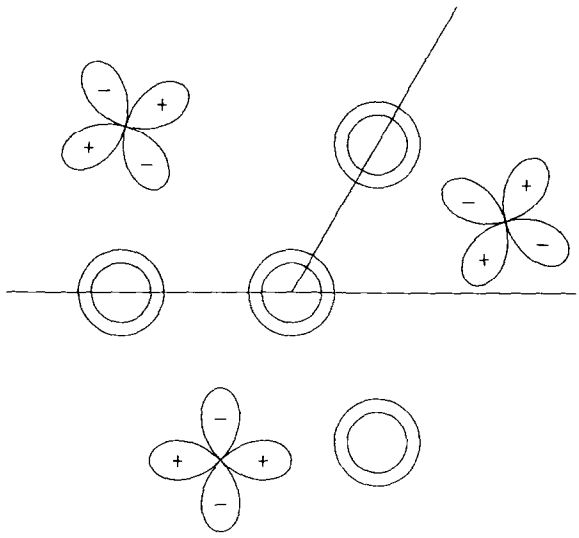

Fig. 19. Schematic diagram showing the grain boundaries of a tri-crystal (100) $SrTiO_3$ substrate and the $YBa_2Cu_3O_{7-\delta}$ epitaxial rings. One ring contains no grain boundary weak links, two contain two, and the ring in the center contains three grain boundary weak links. The $d_{x^2-y^2}$ orbitals are oriented along the a–b axes of the YBCO films and illustrate how the three grain boundary ring is frustrated (from [98]).

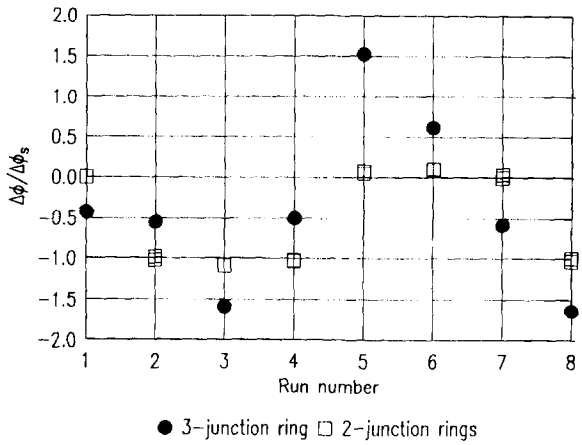

Fig. 20. A scanning SQUID microscope is used to measure the flux through the rings. The open squares near multiples of $hc/2e$ correspond to the trapped flux measured in the 0- and 2-junction rings. The solid points near $(n + \frac{1}{2})(hc/2e)$ correspond to the observed flux in the 3-junction ring (from [98]).

$hc/2e$.

Using a scanning SQUID microscope, Tsuei et al. measured the magnetic flux trapped in the rings when they were cooled from above T_c to 4.2 K in a nearly vanishing external magnetic field. They observed the results shown in Fig. 20. In all cases the two-junction control rings were found to have the same number of flux quanta threading them. The difference between the 2-junction and 0-junction rings was always near to an integer value of $\Phi_0 = hc/2e$, while the difference between the 3-junction ring was always close to $(n + \frac{1}{2})\Phi_0$, as shown in Fig. 20.

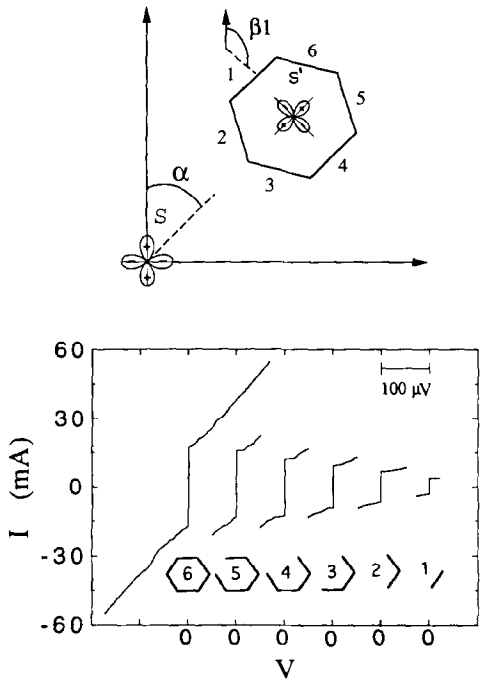

Fig. 21. (a) A schematic representation showing the orientation of the hexagonal superconducting grain S' relative to the rest of the film S. (b) Current-voltage characteristics of a full hexagon and with successive faces removed (from [103]).

There is of course an alternate explanation of this observation in which magnetic spin-flip scattering at a grain boundary induces a π phase shift [100,101]. This was in fact suggested as a possible explanation of the paramagnetic Meissner (Wohlleben) effect [102]. However, both the Wohlleben effect and the half-flux quantum spontaneous magnetization of the three-grain boundary find a natural explanation within the $d_{x^2-y^2}$ picture.

There are, however, other grain boundary and Josephson tunnel junction experiments which raise questions regarding the $d_{x^2-y^2}$ picture. Chaudhari and Lin [103] have reported critical current measurements between two superconducting grains S' and S, schematically illustrated in Fig. 21(a). If the gap has $d_{x^2-y^2}$ symmetry and the pair phase is constant in each region, the Josephson critical current across a given face of the S' hexagon has been argued [99] to vary as

$$I_c = I_1 \cos 2(\alpha - \beta_i) \cos 2\beta_i. \tag{32}$$

Here I_1 is a constant, $\alpha = 45°$, and β_i depends upon the orientation of the grain boundary face as shown in Fig. 21. In the experiment current flows from a contact on the hexagon S' to the outside superconductor S. If the gap has $d_{x^2-y^2}$ symmetry, the magnitude and direction of current flow changes for the different faces according to Eq. (32). Interference between the currents flowing across the different faces implies that if the pair phase is constant in each grain, the sum of the critical currents over all six faces will in fact vanish. In this case, if one of the faces is removed by laser ablation, then the interference will be incomplete and a non-vanishing critical current will be observed. In the experiment a finite critical current was observed, Fig. 21(b), which was directly proportional to

the number of faces present. No interference effects were observed, and it was concluded that these results were consistent with a gap having s-wave symmetry.

However, as discussed by Millis [104], the pair phase need not be constant within each grain. In fact, spontaneous currents will flow such that the free energy is minimized (just as in the case of the three-grain boundary ring discussed above). Thus, it is possible that spontaneous supercurrents flow, creating both magnetic field and kinetic inductance phase shifts

$$\varphi_2 - \varphi_1 = \int_1^2 dx \cdot \left(2mv + \frac{2e}{c}A\right)$$

that give rise to the critical currents which are observed. However, even allowing for this, the observation of a finite critical current across a 45° grain boundary interface is difficult to understand within the $d_{x^2-y^2}$ framework. Like the corner Josephson junction in zero applied field discussed above, a 45° grain boundary would not appear capable of supporting a finite critical current.

One could also envision testing the symmetry of the high-T_c cuprate superconducting order parameter by studying the Josephson tunneling between a conventional s-wave superconductor and a c-axis oriented cuprate superconductor. Sun et al. [105] have in fact observed Josephson tunneling currents in Pb/insulator/$Y_{1-x}Pr_xBa_2Cu_3O_{7-\delta}$ c-axis oriented tunnel junctions. The value of the Josephson current was typically a factor of order 10 smaller than the Ambegaokar-Baratoff [106] value. Nevertheless, it is difficult to understand how there can be a finite critical current along the c-axis if YBCO is a superconductor with $d_{x^2-y^2}$ symmetry. One might argue that YBCO is orthorhombic and not tetragonal, so that the in-plane distortion could admix some s-wave component. However, the experiments have been done on highly twinned crystals, and the critical current is proportional to the area of the junction rather than the square root of the area. Whether currents flowing in the ab plane at steps or etch pits can provide an explanation consistent with a $d_{x^2-y^2}$ gap remains uncertain.

To summarize this discussion as to how we would know if the gap has $d_{x^2-y^2}$ symmetry:

- 1. Power law behavior of the low-temperature transport properties such as the penetration depth, the Knight shift, and the nuclear relaxation rate T_1^{-1} are consistent with a $d_{x^2-y^2}$ gap. Furthermore, the behavior of these quantities with impurities can be understood within the framework of a dirty $d_{x^2-y^2}$-wave model. Raman scattering and inelastic neutron scattering can also be described within this phenomenology.
- 2. ARPES measurements find evidence for a highly anisotropic gap, consistent with a $d_{x^2-y^2}$ gap.
- 3. SQUID interference experiments, corner Josephson junction studies, and flux quantization measurements in grain boundary rings can be interpreted in terms of a $d_{x^2-y^2}$ gap.

However, there are other experiments which raise questions regarding the existence of a $d_{x^2-y^2}$ gap, such as the Chaudhari-Lin experiment [103] on interfacial tunneling and the Sun et al. [105] c-axis Pb–YBCO Josephson current work. In addition, the temperature dependence of both the penetration depth and surface resistance of the "electron-doped" cuprate $Nd_{2-x}Ce_xCuO_4$ appear to follow the BCS s-wave expressions [107]. Beyond this, the relationship of the residual resistance to the observed shift in T_c for $Y_{1-x}Pr_xCu_3O_7$ and irradiated YBCO samples raise questions as to whether a $d_{x^2-y^2}$ gap is possible [108]. Is this a lifetime or carrier density problem? Finally, the isotope effect [109] also poses an important challenge to our understanding of these materials.

4. Conclusions

At the past March (1994) APS meeting, Barbara Levi asked Bertram Batlogg "When do you think we'll have a definitive experiment on the symmetry of the gap?" Batlogg answered, "We already have. It's just that we don't all agree on which experiment it is." Further experiments will help clarify this. In particular, different experiments on the same samples can provide important constraints on the theoretical interpretations. For example, in recent specific heat measurements [110] of $YBa_2Cu_3O_{6.95}$ crystals in the presence of a c-axis magnetic field H, the coefficient of the linear term in the specific heat was observed to vary as $H^{1/2}$ (see Fig. 22). This behavior was predicted by Volovik [111] for a gap with nodes. He showed that the quasi-particle spectrum is shifted by the superfluid velocity around a vortex core resulting in an effective quasi-particle density of states proportional to $(H/H_{c2})^{1/2}$. The fact that these crystals were grown by the same technique [112] as those which showed a linear temperature dependence of the penetration depth [69] provides the possibility of comparing predictions for a given model. In this case the magnitudes of the effects are consistent with a $d_{x^2-y^2}$ gap. Another example is the measurement of the real and imaginary parts of the surface impedance of YBCO crystals. This provides data on the real part of the conductivity [57] σ_1 and the penetration depth [69] λ. Calculations [113] of σ have been carried out using a dirty-$d_{x^2-y^2}$-wave model. When the gap Δ_0 and scattering rate Γ are adjusted to fit the penetration depth data, one can check to see how well the theory fits the σ_1 data. What is found is that while some features of the experimental σ_1 data are reproduced, the present theory predicts that at low temperatures σ_1 has a T^2 temperature dependence while the experiment appears to exhibit a linear T variation. Thus further work is needed. Perhaps NMR as well as ARPES studies for these same crystals could also be carried out. It will also be important to determine if other cuprates exhibit $(n+\frac{1}{2})(hc/2e)$ flux trapping in the three-grain boundary ring experiment. In particular, what about the "electron doped" cuprate $Nd_{2-x}Ce_xCuO_4$ which appears to have a BCS s-wave temperature dependence for λ and the surface resistance. [107]

On the theory side, there also remain a number of issues. At the phenomenological level, calcula-

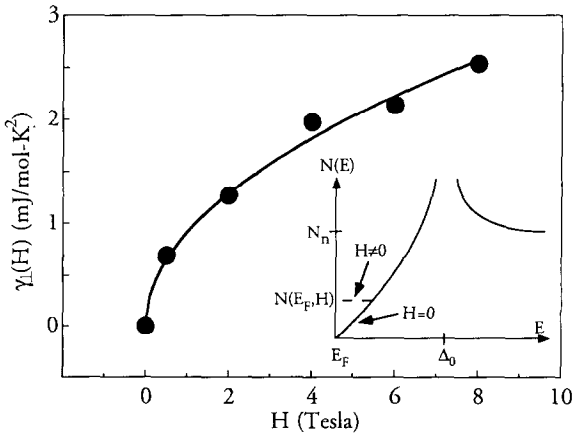

Fig. 22. The coefficient of the field-dependent linear temperature contribution to the specific heat $\gamma_\perp(H)$ versus H for a single crystal of $YBa_2Cu_3O_{6.95}$. The solid line is a fit to $\gamma_\perp(H) = AH^{1/2}$ with $A = 0.91$ mJ/mol-K^2-$T^{1/2}$ as predicted for lines of nodes. The inset shows a schematic density of states. From Ref. [110].

tions of a range of properties can provide more stringent tests of the theory. In addition, experimental input such as the recent neutron scattering results [114–116,90] for $La_{2-x}Sr_xCuO_4$ provide a basis for testing theoretical ideas. For example, such data [114] have been used to determine the NMR relaxation [117] times for Cu and O. The analysis in fact suggests that there are difficulties in understanding the O relaxation within the usual one-component framework. It should also be possible with the availability of higher energy neutron scattering data [118] to determine whether there is sufficient coupling strength in the spin-fluctuation spectrum [119] to offer the possibility for producing the observed T_c. Here of course the absence of a Migdal theorem limits this type of analysis, but it can nevertheless offer useful qualitative information.

Finally, there remains the nagging feeling that even if the basic pairing mechanism ultimately arises from the short-range antiferromagnetic correlations in a CuO_2 layer, some important ingredient may be missing from the theory we have described. For example, perhaps frustration [120] of the Cu–Cu exchange coupling which can occur when a hole is on the O site between the Cu's plays a critical role. Is this frustration responsible for the spin-gap behavior [121] observed in some cuprates? Could it be important for a system to "almost" exhibit a spin gap in order to have a high transition temperature [122,123]? Within the antiferromagnetic spin-fluctuation exchange theory we have discussed, one finds that if the spin fluctuation spectral weight at energies less than $2\Delta_0$ could simply be moved to energies greater than $2\Delta_0$ without altering its strength, T_c would be enhanced [124] [4]. Presently work on the doped two-chain Hubbard model [126], which exhibits a spin gap, offers the possibility of numerically exploring the pair-field correlations in a system which has a spin gap. There are of course many other theoretical suggestions regarding the essential ingredients, so that just as in the case of the experimental studies, there is at present no consensus, and the case for spin-fluctuation mediated $d_{x^2-y^2}$ pairing in the cuprates remains open.

Acknowledgments

The work on the effective interaction in the Hubbard model which is described here was carried out with N. Bulut and S.R. White. I have also been fortunate to interact with a wonderful group of students and postdocs, some of whose contributions have been referenced here. The ideas discussed here also owe a great deal to early discussions of the magnetic properties of the cuprates with C. Hammel, R. Heffner, Z. Fiske, J. Smith, and M. Takigawa; and I would like to acknowledge the Program on Correlated Electrons at the Center for Materials Science at Los Alamos National Laboratory. In addition, I would like to thank G. Aeppli, B. Batlogg, M. Beasley, R. Birgeneau, D. Bonn, P. Chaudhari, R. Dynes, W. Hardy, J. Kirtley, Z.X. Shen, C. Slichter, D. Van Harlingen, and R. Walstedt for insightful discussions and help in understanding their beautiful experiments. I would also like to thank E. Abrahams, J.R. Schrieffer, and C.M. Varma for their helpful comments. This work was supported by the National Science Foundation under grant DMR92–25027 and the Department of Energy under grant DE–FG03–85ER45197. The computations were carried out at the San Diego Supercomputer Center and the National Energy Research Supercomputing Center.

[4] The reduction of T_c in the cuprates produced by dynamic pair breaking arising from Coulomb interactions was originally suggested by P.A. Lee and N. Read [125].

Appendix A

Prior to the discovery of the high-temperature superconductors, the Hubbard model was being studied in connection with various organic as well as heavy-fermion materials. The possibility that spin-density wave fluctuations in weakly coupled chains could lead to pairing was raised in connection with the observation of superconductivity in the Bechgaard salts [167]. Numerical simulations of the Hubbard model suggested that there could be an attractive near-neighbor pairing interaction [127]. Motivated by the discovery of superconductivity in UBe_{13} and UPt_3 [128], phenomenological [129] and diagrammatic RPA calculations [130] found that near an antiferromagnetic instability the exchange of spin-fluctuations could lead to $d_{x^2-y^2}$ pairing.

Following the discovery of the cuprate superconductors, the possibility of antiferromagnetic paramagnon mediated pairing was discussed for a nearly half-filled 2D Hubbard model [131,132]. Using an RPA approximation for the effective electron-electron interaction, Eq. (12), the Eliashberg $d_{x^2-y^2}$ coupling strength[5]

$$\lambda_{d_{x^2-y^2}} = \frac{\langle g_{d_{x^2-y^2}}(p') V_{\rm eff}(p'-p,\omega=0) g_{d_{x^2-y^2}}(p)\rangle}{\langle g^2_{d_{x^2-y^2}}(p)\rangle}, \tag{A.1}$$

with $g_{d_{x^2-y^2}}(p) = (\cos p_x - \cos p_y)$ was studied as a function of U and the band filling. The averages were taken over the Fermi surface of the 2D system with $\varepsilon_p = -2t(\cos p_x + \cos p_y) - \mu$. A similar calculation of the wave function renormalization factor λ_z was also carried out giving an effective coupling $\lambda_{d_{x^2-y^2}}/(1+\lambda_z)$. Combined with the average interaction frequency $\langle\omega\rangle$, the resulting estimate for the transition temperature was encouraging. However, the linear T dependence predicted for the low-temperature penetration depth of a $d_{x^2-y^2}$ superconductor appeared to be in disagreement with early μsr [133] and magnetization measurements [134].

In the large U limit, a canonical transformation of the Hubbard model in which terms of order t^2/U are kept, leads to the t–J model

$$\begin{aligned}\tilde{H} = &-t\sum_{\langle ij\rangle,\sigma}(c^\dagger_{i\sigma}c_{j\sigma} + c^\dagger_{j\sigma}c_{i\sigma}) + J\sum_{\langle ij\rangle}(\boldsymbol{s}_i\cdot\boldsymbol{s}_j - \tfrac{1}{4}n_in_j)\\ &-\tfrac{1}{4}J\sum_{i,r\neq r',\sigma}(c^\dagger_{i+r,\sigma}c^\dagger_{i,-\sigma}c_{i,-\sigma}c_{i+r',\sigma} + c^\dagger_{i+r,-\sigma}c^\dagger_{i,\sigma}c_{i,-\sigma}c_{i+r',\sigma}).\end{aligned} \tag{A.2}$$

Here the exchange interaction $J = 4t^2/U$ and it is understood that $\tilde{H}$ acts in a Hilbert space where double occupancy of a site is forbidden. The third term is a three-site hopping interaction which is proportional to J times the hole density per site x and is often neglected near half-filling. Gros et al.[135] used a Gutzwiller–BCS variational wavefunction $|\Phi\rangle$ to study the ground state of the t–J model with

[5] It might be thought that this calculation neglects retardation because it involves an average over the Fermi surface of $V_{\rm eff}(p'-p,\omega=0)$. However, the point is that $\int_0^\infty (d\omega/\pi)2{\rm Im}V_{\rm eff}(p'-p,\omega)/\omega = V_{\rm eff}(p'-p,\omega=0)$, so that the frequency dependence of the interaction is included in the same manner as the familiar electron-phonon problem in which $\lambda = \int_0^\infty d\omega 2\alpha^2F(\omega)/\omega$. This of course only gives a measure of the strength of the interaction and to determine T_c within the Eliashberg framework it is necessary to keep the full momentum and frequency dependence of the interaction as discussed in [148,46].

$$|\Phi\rangle = \prod_i (1 - n_{i\uparrow} n_{i\downarrow}) \prod_k (u_k + v_k c^\dagger_{k\uparrow} c^\dagger_{-k\downarrow})|0\rangle. \tag{A.3}$$

The first term projects out all doubly occupied sites of the BCS-like state. Taking

$$\frac{v_k}{u_k} = \frac{\Delta_k}{\varepsilon_k + \sqrt{\varepsilon_k^2 + \Delta_k^2}}, \tag{A.4}$$

with $\varepsilon_k = -2t(\cos k_x + \cos k_y) - \mu$, they calculated the groundstate energy $\langle\Phi|\tilde{H}|\Phi\rangle$ for various choices of Δ_k. For the nearly half-filled band, they found that the $d_{x^2-y^2}$ gap, $\Delta_k = \Delta_0(\cos k_x - \cos k_y)$ gave the lowest variational energy. A similar conclusion, that hole doping of the t–J model leads to a $d_{x^2-y^2}$ ground state, was found in auxiliary-boson mean-field treatments [136,137]. At larger dopings $x > 0.1$, Li et al.[138], keeping the three-site interaction, found that the mixed $s^* + id_{x^2-y^2}$ state gave the lowest variational ground state energy.

Phenomenological arguments based upon the notion that the superexchange interaction along with possible second- and third-neighbor phonon interactions could give rise to $d_{x^2-y^2}$ pairing were also proposed [139]. Recently it has been suggested [140] that this superexchange interaction is related to the exchange of spin-fluctuations and arises from the virtual exchange of high-energy spin excitations across the lower and upper Hubbard bands. Dzyaloshinskii [141] and Schulz [142] independently carried out weak-coupling renormalization group calculations for the two-dimensional Hubbard model which took into account the effect of the Van Hove singularity and led to $d_{x^2-y^2}$ pairing. Dzyaloshinskii and Yakovenko [143] found that for a more general interaction the renormalization group equations could lead to various instabilities including single superconducting $d_{x^2-y^2}$ pairing, along with possible coherent mixtures of CDW and SDW phases. Ruvalds [144] and co-workers also found that $d_{x^2-y^2}$ pairing was favored for nested Fermi surfaces consisting of nearly parallel orbit segments.

In the spin bag picture proposed by Schrieffer, Wen, and Zhang [145], an added hole locally weakens the antiferromagnetic correlations, creating a region which can be shared by another hole. This approach leads to s or $d_{x^2-y^2}$ pairing, depending upon whether the dominant momentum transfers are small or large. They also suggested the possibility that nodeless d-wave pairing could occur if the Fermi surface consisted of separate regions near the X–Y points of the Brillouin zone. Kampf and Schrieffer [146] showed how the spin-bag mechanism could arise from cross-line diagrams in the paramagnetic metallic phase of the doped Hubbard model. Frenkel and Hanke [147] discussed the role of transverse spin-fluctuations and their contribution to pairing in the spin-bag model.

In order to go beyond the earlier calculations of the Eliashberg coupling parameters, Bickers et al. [148,149] carried out a conserving, self-consistent, fluctuation exchange approximation calculation for a two-dimensional Hubbard model. In this approach, the propagators are generated from a free-energy functional consisting of particle-particle ladder and particle-hole ladder and bubble skeleton graphs. The single-particle Green's function which enters these graphs is fully dressed and all the momentum and Matsubara frequency dependencies are kept. One merit of this approach is that relevant Ward identities are satisfied so that conservation laws for particle number, momentum and energy are automatically satisfied. In addition the influence of self-energy effects on the particle-particle pairing instability as well as on the spin-fluctuations which drive it are included. This approach does neglect vertex corrections and the cross-line diagrams of the spin-bag model. Calculations of these corrections [150,151] suggest that they are small for weak-to-moderate coupling. In addition, the results obtained from the conserving approximation were shown to be in reasonable agreement with available Monte

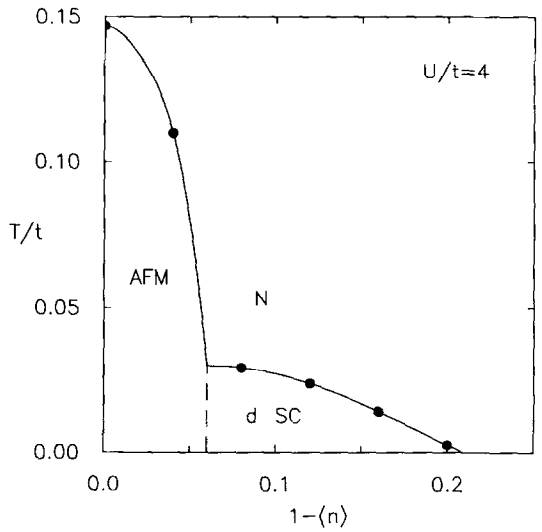

Fig. 23. Phase diagram for a doped two-dimensional Hubbard model with $U/t = 4$ calculated within a conserving, fluctuation exchange approximation.

Carlo data at higher temperatures [148,149]. As seen in Fig. 23, the conserving approximation calculations showed that when the two-dimensional Hubbard model was doped beyond a critical doping, the leading instability changed from the SDW channel to the $d_{x^2-y^2}$ pairing channel. For $U = 4t$ and a doping of $x = 0.15$, a superconducting transition temperature of order $0.02t$, which for a bandwidth $8t = 2$ eV corresponds to 60 K, was obtained. Recently, this approach has been extended to treat the superconducting state [39,40] at temperatures below T_c. The simple $(\cos p_x - \cos p_y)$ form was found to provide an excellent fit of the angular dependence of the dressed gap $\Delta(p, i\pi T)$ on the Fermi surface. In addition, the maximum value of the gap antinode at low temperatures $\Delta_0(0)$ was found to give a $2\Delta_0(0)/kT_c$ value of order 8 to 10. These calculations also showed the importance of nonlinear feedback effects, which arise in the conserving approximation, in stabilizing the strength of the spin-fluctuation pairing interaction below T_c.

Within a phenomenological framework, antiferromagnetic spin fluctuations provide an approach for interpreting the unusual normal state NMR relaxation rates [47–51] and the electrical conductivity of the cuprates [152,46]. Using an RPA-like parameterization [49] of the spin susceptibility which fit the NMR data and a coupling strength consistent with the observed resistivity, Monthoux and Pines [46,153] carried out an Eliashberg-like calculation and obtained a transition temperature consistent with that observed in the high-T_c cuprates. In these calculations, just as in the conserving approximation, the full momentum and Matsubara frequency dependencies of the interaction were taken into account. Similar calculations leading to high T_c values using a self-consistent renormalization theory of spin-fluctuations were carried out by Moriya [152,154] and co-workers. Radtke et al.[119] have also solved the Eliashberg equations with an interaction in which χ was parameterized to fit the available neutron scattering data but found T_c values of only 10 to 20 K.

In addition to these diagrammatic and phenomenological approaches, there has been a variety of numerical calculations aimed at obtaining exact results. For example, Lanczos diagonalization calculations for small clusters have been carried out for both the t–J model [155,44,156,157] and the Hubbard model [65]. In the former, diagonalization of clusters with up to 26 sites shows that a critical

threshold value of J/t exists above which the two holes are bound. That is, the energy of two 26-site clusters in which two holes are added to one of the clusters is lower than if one hole is added to each cluster. This critical value of J/t is estimated to be of order 0.3. The state of the undoped 26-site system has s-wave symmetry, while the 2-hole ground state has $d_{x^2-y^2}$ symmetry. These results are in agreement with Green's function Monte Carlo simulations [158] on larger lattices which estimate that two holes will bind on an infinite lattice if $J/t \gtrsim 0.27$. However, the binding energy on the infinite lattice is significantly reduced ($0.1\,t$ for $J/t = 0.4$) from that found on a $4 \times 4 (0.349\,t)$ lattice. While it has been suggested that phase separation [43] will take place for any finite value of J/t, this is in disagreement with the interpretation of results obtained from exact diagonalization studies [159] and high-temperature expansions [160] which conclude that phase separation does not occur for $J/t < 1$.

Exact diagonalization studies of the Hubbard model on 4×4 lattices [65] find that for $U/t > 3$, two holes added to the half-filled cluster are bound (i.e. $E_0(14) - E_0(16) - 2E_0(15) < 0$). The symmetry of the two-hole ground state is $d_{x^2-y^2}$ relative to the ground state of the half-filled system. However, whether the binding energy remains finite or vanishes as the lattice size increases is not known. It is however found that two holes added to a two-chain Hubbard model bind in a $d_{x^2-y^2}$-like state [126].

Monte Carlo simulations have provided insight into the physical properties of the two-dimensional Hubbard model [161,162]. A number of normal state properties ranging from the long-range antiferromagnetic order of the half-filled ground state to the $|1 - \langle n \rangle|$ variation of the Drude weight of the doped system are consistent with experimental observations on the cuprates. In addition, Monte Carlo calculations have shown that the particle-particle interaction in the $d_{x^2-y^2}$ channel is attractive near half-filling [163,164]. However, finite-temperature Monte Carlo [62] simulations on 8×8 lattices with $U/t = 4$ and $T = t/6$ as well as "zero temperature" projector Monte Carlo calculations on 12×12 lattices [61] find that the equal time $d_{x^2-y^2}$ and extended s-wave pair field correlation functions remain very short range even when the lattice is doped near half-filling. In addition, calculations of the Drude weight and the superfluid density find that while the Drude weight of the doped Hubbard model is finite, implying that it is metallic, no superfluid density was observed at the temperatures ($T = 0.25\,t$) and lattice sizes (12×12) that could be reached [63,64].

Recent density matrix numerical renormalization calculations of the ground state of the two-chain Hubbard model find power law $d_{x^2-y^2}$-like pair-field correlations which, as shown in Fig. 24, are enhanced by an on-site Coulomb interaction [126]. This could mean that previous Monte Carlo simulations for the doped two-dimensional Hubbard model simply failed to reach sufficiently low temperatures to see the development of long-range pair-field correlations. However, it could also mean that the spin gap, which occurs in a two-chain Hubbard model, is an essential ingredient. Just as in the case of the experimental studies of the cuprates, further theoretical work is needed.

Appendix B

This paper originated from several Colloquia which I gave during the spring quarter of 1994. The idea was to discuss why the superconducting state of the cuprates might have $d_{x^2-y^2}$ symmetry and how this could be tested experimentally. Some background regarding what is meant by $d_{x^2-y^2}$ symmetry follows.

Shortly after Bednorz and Muller's discovery [1] of superconductivity in $La_{2-x}Ba_xCuO_4$, Shapiro

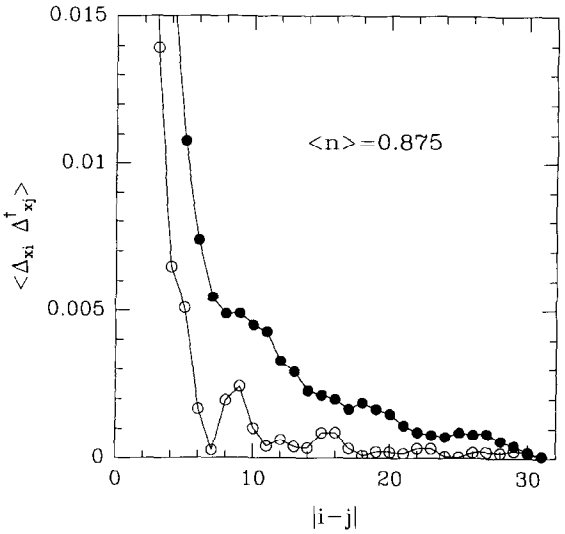

Fig. 24. The equal-time rung-rung singlet pair-field correlation function $\langle \Delta_i \Delta_j^+ \rangle$ for a 2×32 Hubbard ladder versus $|i-j|$. Here Δ_j^+ creates a single pair across the rung of a two-chain Hubbard ladder doped so that $\langle n \rangle = 0.875$. The ladder is characterized a one-electron hopping t along each chain and a hopping $t_\perp = 1.5t$ across the rungs connecting the chains. This ground state calculation represents, to our knowledge, the first numerical evidence that the range of pair-field correlations can be enhanced in a Hubbard model by the presence of U ($U = 8$ solid circles and $U = 0$ open circles). From R. Noack et al., Ref. [126]

step [67] and flux quantization [68] measurements confirmed that the superconducting phase was indeed the usual BCS $2e$ charged pair condensate. In addition, Knight shift measurements [16,17] showed a vanishing spin susceptibility so the pairs were determined to be in a singlet state. Thus we know that the condensate can be described by the pair wave function [165]

$$ {}_{N-2}\langle \psi_{s_1}(x_1)\psi_{s_2}(x_2)\rangle_N = \varphi(x_1 - x_2)e^{-iP_{cm}(x_1+x_2)/2}\frac{(\alpha_1\beta_2 - \beta_1\alpha_2)}{\sqrt{2}}. \tag{B.1}$$

Here $\psi_{s_1}(x_1)$ destroys an electron of spin s_1 at position x_1, and the expectation value is taken between the ground states of N and $N-2$ particles. The center of mass pair phase of the second term on the right-hand side of in Eq. (B.1) describes the usual superfluid properties, while the relative coordinate wave function $\varphi(x_1 - x_2)$ describes the orbital symmetry of the pairs[6]. In a rotationally symmetric system, φ can be expanded in spherical harmonics, and for a singlet state one would speak of s, d, ... orbital symmetry. In a planar lattice with D_{4h} symmetry one has the five even parity representations listed in Table 1. Now, one can express $\varphi(x_1 - x_2)$ in k-space so that

$$\varphi(x_1 - x_2) = \sum_k \varphi_k e^{i\mathbf{k}\cdot(\mathbf{x}_1 - \mathbf{x}_2)}. \tag{B.2}$$

Then using the simplest basis functions of a given representation, we speak of a Cooper pair with

[6] In general the fermion field operators $\psi_s(x)$ can also depend on the time leading to a φ which depends upon $t_1 - t_2$. This is reflected in the frequency dependence of the gap.

extended s-wave symmetry if $\varphi_k \sim (\cos k_x + \cos k_y)$ or $d_{x^2-y^2}$-wave symmetry if $\varphi_k \sim (\cos k_x - \cos k_y)$.

Physically, in a superconductor, the quasi-particles interact with the pair condensate so that the gap Δ_k in the quasi-particle spectrum is related to φ_k. The BCS theory [166] tells us that

$$\varphi_k = \Delta_k / E_k, \tag{B.3}$$

with $E_k = \sqrt{\varepsilon_k^2 + \Delta_k^2}$, and Δ_k given by

$$\Delta_k = -\sum_{k'} \frac{V_{kk'}\Delta_{k'}}{2E_{k'}}. \tag{B.4}$$

This can be rewritten, using Eq. (B.3), as a wave equation for φ_k,

$$2E_k\varphi_k + \sum_{k'} V_{kk'}\varphi_{k'} = 0. \tag{B.5}$$

Here the eigenvalue is zero, corresponding to placing the pairs at the chemical potential.

Thus we see that the symmetry of φ_k reflects the symmetry of the interaction. Furthermore, when one speaks of the gap Δ_k as having $d_{x^2-y^2}$ symmetry, one is also saying that the relative coordinate wave function of the pairs φ_k has $d_{x^2-y^2}$ symmetry.

References

[1] J.G. Bednorz and K.A. Muller, Z. Phys. B 64 (1986) 189.
[2] A. Schilling, M. Cantoni, J.D. Guo, and H.R. Ott, Nature 362 (1993) 56.
[3] Physical Properties of High Temperature Superconductors, Vol. 1–4, D.M. Ginzberg (World Scientific, Singapore).
[4] High Temperature Superconductivity Proceedings, The Los Alamos Symposium (Addison Wesley, 1989).
[5] B. Batlogg, Physics Today (June 1991) p. 44.
[6] See, for example, J. Phys. Chem. Solids, 54, No. 10 (1993).
[7] B. Keimer et al., Phys. Rev. B 46 (1992) 14034.
[8] J. Zaanen, G.A. Sawatzky, and J.W. Allen, Phys. Rev. Lett. 55 (1985) 418.
[9] W.E. Pickett, Rev. Mod. Phys. 61 (1989) 433.
[10] C.M. Varma, S. Schmitt-Rink, and E. Abrahams, Solid State Comm. 62 (1987) 681.
[11] D.S. Rokhsar, Phys. Rev. Lett. 70 (1993) 493.
[12] R.B. Laughlin, Proc. Summer School on Modern Perspectives in Many-Body Physics, Canberra, Jan. 1993 (World Scientific, Singapore).
[13] P.W. Anderson, in Superconductivity, Proc. ICTP Spring College, (1992), P. Butcher and Y. Lu, eds. (World Scientific, Singapore).
[14] S. Chakravarty, A. Sudbo, P.W. Anderson, and S. Strong, Science 261 (1993) 337.
[15] Y. Guo et al., Science, 239, 896 (1988);
G. Chen and W.A. Goddard, Science 239 (1988) 899.
[16] S.E. Barrett et al., Phys. Rev. Lett. 66, 108 (1991); Phys. Rev. B 41 (1990) 6283.
[17] M. Takigawa, P.C. Hammel, R.H. Heffner, and Z. Fisk, Phys. Rev. B 39 (1989) 7371.
[18] S. Kamal et al., Phys. Rev. Lett., in press.
[19] G. Mozurkewich et al., Phys. Rev. B 46 (1992) 11914.
[20] M. Sigrist and T.M. Rice, Z. Phys. B 68 (1987) 9.
[21] L. Chen and A.-M.S. Tremblay, J. Phys. Chem. Solids, 54 (1993) 1381.
[22] V.J. Emery, Phys. Rev. Lett. 58 (1988) 2794.

[23] F.C. Zhang and T.M. Rice, Phys. Rev. B 37 (1988) 3759.
[24] M.S. Hybertsen, M. Schluter, and N.E. Christensen, Phys. Rev. B 39 (1989) 9028.
[25] J.F. Annett and R.M. Martin, Phys. Rev. B 42 (1990) 3929.
[26] O.K. Anderson et al., Phys. Rev. B 49 (1994) 4195.
[27] J. Hubbard, Proc. R. Soc. London, Ser. A 243 (1957) 336.
[28] G. Dopf, A. Muramatsu, and W. Hanke, Phys. Rev. B 41 (1990) 9264; Phys. Rev. Lett. 68 (1992) 353.
[29] R.T. Scalettar, D.J. Scalapino, R.L. Sugar and S.R. White, Phys. Rev. B 44 (1991) 770.
[30] A.P. Kampf, Physics Reports 249 (1994) 219;
W. Brenig, Physics Reports 251 (1995) 153.
[31] J.E. Hirsch and S. Tang, Phys. Rev. Lett. 62 (1989) 591.
[32] S.R. White et al., Phys. Rev. B 40 (1989) 506.
[33] A. Moreo et al., Phys. Rev. B 41 (1990) 2313.
[34] L. Chen, C. Bourbonnais, T. Li, and A.-M.S. Tremblay, Phys. Rev. Lett. 66 (1991) 369.
[35] N. Bulut, D.J. Scalapino and S.R. White, Phys. Rev. B 47 (1993) 2742.
[36] N.F. Berk and J.R. Schrieffer, Phys. Rev. Lett. 17 (1966) 433; Phys. Rev. B 30 (1966) 1408.
[37] N. Bulut, D.J. Scalapino and S.R. White, Phys. Rev. B 47 (1993) 6157.
[38] N. Bulut, D.J. Scalapino and S.R. White, Phys. Rev. B 47 (1993) 14599.
[39] Chien-Hua Pao and N.E. Bickers, Phys. Rev. Lett. 72 (1994) 1870.
[40] P. Monthoux and D.J. Scalapino, Phys. Rev. Lett. 72 (1994) 1874.
[41] G.M. Eliashberg, Soviet Phys. JETP 11 (1960) 696.
[42] P. Morel and P.W. Anderson, Phys. Rev. 125 (1962) 1263.
[43] V.J. Emery, S.A. Kivelson, and H.Q. Lin, Phys. Rev. Lett. 64 (1990) 475.
[44] D. Poilblanc, J. Riera and E. Dagotto, Phys. Rev. B 43 (1991) 7899;
D. Poilblanc, Phys. Rev. B 49 (1994) 1477.
[45] T. Moriya, Y. Takahashi, and K. Ueda, J. Phys. Soc. Japan 59 (1990) 2905.
[46] P. Monthoux and D. Pines, Phys. Rev. Lett. 69 (1992) 961; Phys. Rev. B 47 (1993) 6069; B 49 (1994) 4261.
[47] B.S. Shastry, Phys. Rev. Lett. 63 (1989) 1288.
[48] N. Bulut, D. Hone, D.J. Scalapino and N.E. Bickers, Phys. Rev. B 41 (1990) 1797; Phys. Rev. Lett. 64 (1990) 2723.
[49] A.J. Millis, H. Monien and D. Pines, Phys. Rev. B 42 (1990) 167.
[50] K. Levin, J.H. Kim, J.P. Lu, and Q. Si, Physica C 175 (1991) 449;
Y. Zha, Q. Si and K. Levin, Physica C 212 (1993) 413.
[51] Q. Si, Y. Zha, K. Levin, and J.P. Lu, Phys. Rev. B 47 (1993) 9055.
[52] T. Ito, K. Takenaka and S. Uchida, Phys. Rev. Lett. 70 (1993) 3995.
[53] J.M. Tranquada et al., Phys. Rev. B 46 (1992) 5561.
[54] J. Rossat-Mignod et al., Physica C 185–189 (1991) 86.
[55] B. Bucher et al., Phys. Rev. Lett. 70 (1993) 2012.
[56] H. Zimmerman et al., Physica C 159 (1989) 681.
[57] D.A. Bonn et al., Phys. Rev. B 47 (1993) 11314.
[58] S.M. Quinlan, D.J. Scalapino and N. Bulut, Phys. Rev. B 49 (1994) 1470.
[59] J. Gleick, Genius (The Life and Science of Richard Feynman) (Pantheon Books, Random House, New York, 1992).
[60] M. Sato et al., J. Phys. Soc. Japan 62 (1993) 263.
[61] M. Imada, J. Phys. Soc. Japan 60 (1991) 2740.
[62] A. Moreo, Phys. Rev. B 45 (1992) 5059.
[63] D.J. Scalapino, S.R. White, and S.C. Zhang, Phys. Rev. Lett. 68 (1992) 2830.
[64] F.F. Assaad, W. Hanke and D.J. Scalapino, Phys. Rev. B 49 (1994) 4327.
[65] G. Fano, F. Ortolani, and A. Parola, Phys. Rev. B 46 (1992) 1048.
[66] E. Dagotto, Rev. Mod. Phys.
[67] D. Esteve et al., Europhys. Lett. 3 (1987) 1237.
[68] P. Gammel et al., Phys. Rev. Lett. 59 (1987) 2592.
[69] W.N. Hardy et al., Phys. Rev. Lett. 70 (1993) 3999.
[70] P.J. Hirschfeld and N. Goldenfeld, Phys. Rev. B 48 (1993) 4219.

[71] J.E. Sonier et al., Phys. Rev. Lett. 72 (1994) 744.
[72] Y. Kitaoka, J. Phys. Soc. Japan, 62, 2803 (1993);
Y. Kitaoka et al., J. Phys. Chem. Solids, 54 (1993) 1385.
[73] T. Hotta, J. Phys. Soc. Japan 62 (1993) 274.
[74] K. Ishida et al., J. Phys. Soc. Japan 62 (1993) 2803.
[75] N. Bulut and D.J. Scalapino, Phys. Rev. Lett. 68 (1992) 706; Phys. Rev. B 45 (1992) 2371.
[76] F. Mila and T.M. Rice, Physica C 157 (1989) 561.
[77] P.C. Hammel, M. Takigawa, R.H. Heffner, Z. Fisk, and K.C. Ott, Phys. Rev. Lett. 63 (1992) (1989).
[78] J.A. Martindale et al., Phys. Rev. Lett. 68 (1992) 702.
[79] T. Imai, T. Shimizu, H. Yasnoka, Y. Ueda and K. Kosuge, J. Phys. Soc. Japan 57 (1988) 2280.
[80] Y. Kitaoka et al., Physica C 153 (1988) 83.
[81] R.E. Walstedt et al., Phys. Rev. B 40 (1989) 2572.
[82] N. Bulut, D.W. Hone, D.J. Scalapino and N.E. Bickers, J. Appl. Phys. 67 (1990) 5079.
[83] M. Takigawa, J.L. Smith and W.L. Hults, Physica C 185 (1991) 1105; Phys. Rev. B 44 (1991) 7764.
[84] J.A. Martindale, S.E. Barrett, K.E. O'Hara, C.P. Slichter, W.C. Lee and D.M. Ginsberg, Phys. Rev. B 47 (1993) 9155.
[85] Y. Itoh et al., J. Phys. Soc. Japan 61 (1992) 1287.
[86] D. Thelen, D. Pines and J.P. Lu, Phys. Rev. B 47 (1993) 9151.
[87] N. Bulut and D.J. Scalapino, Phys. Rev. Lett. 67 (1991) 2898.
[88] T.P. Devereaux et al., Phys. Rev. Lett. 72 (1994) 396.
[89] M.C. Krantz and M. Cardona, Phys. Rev. Lett. 72 (1994) 3290;
see also T.P. Devereaux et al., Phys. Rev. Lett. 72 (1994) 3291.
[90] T.E. Mason et al., Phys. Rev. Lett. 71 (1993) 919.
[91] S.M. Quinlan and D.J. Scalapino, Phys. Rev. B, to appear.
[92] D. Pines, private communication.
[93] Z.-X. Shen and D.S. Dessau, Physics Reports, to appear.
[94] Z.-X. Shen et al., Phys. Rev. Lett. 70, 1553 (1993); J. Chem. Solids 54 (1993) 1169.
[95] D.A. Wollman et al., Phys. Rev. Lett. 71 (1993) 2134.
[96] R.A. Klemm, preprint.
[97] See for example D.A. Brawner and H.R. Ott, preprint.
[98] C.C. Tsuei et al., Phys. Rev. Lett. 73 (1994) 593.
[99] M. Sigrist and T.M. Rice, J. Phys. Soc. Japan 61 (1992) 4283.
[100] L.N. Bulaevskii, V.V. Kuzii and A.A. Sobyanin, Sov. Phys. JEPT Lett. 25 (1977) 290.
[101] B.I. Spivak and S.A. Kivelson, Phys. Rev. B 43 (1991) 3740.
[102] W. Braunisch et al., Phys. Rev. Lett. 68 (1992) 1909.
[103] P. Chaudhari and Lin, Phys. Rev. Lett. 72 (1994) 1084.
[104] A.J. Millis, Phys. Rev. B 49 (1994) 15408.
[105] A.G. Sun, D.A. Gajewski, M.B. Maple, and R.C. Dynes, Phys. Rev. Lett. 72 (1994) 2267.
[106] V. Ambegaokar and A. Baratoff, Phys. Rev. Lett. 10 (1963) 486.
[107] Dong Ho Wu et al., Phys. Rev. Lett. 70 (1993) 85.
[108] R.C. Dynes, private communication.
[109] J.P. Franck, in Physical Properties of High T_c Superconductors IV, D.M. Ginsberg, ed. (World Scientific, 1994) 189.
[110] K.A. Moler et al., preprint.
[111] G.E. Volovik, JETP 58 (1993) 469.
[112] R. Liang et al., Physica C 195 (1992) 51.
[113] P.J. Hirschfeld, W.O. Putikka, and D.J. Scalapino, Phys. Rev. B.
[114] S.-W. Cheong et al., Phys. Rev. Lett. 67 (1991) 1791.
[115] T.R. Thurston et al., Phys. Rev. B 46 (1992) 9128.
[116] M. Matsuda et al., J. Phys. Soc. Japan 62 (1993) 443.
[117] R.E. Walstedt, B.S. Shastry and S.-W. Cheong, preprint.
[118] G. Aeppli, private communication.
[119] R.J. Radtke, S. Ullah, K. Levin and M.R. Norman, Phys. Rev. B 46 (1992) 11975.

[120] A. Aharony et al., Phys. Rev. Lett. 60 (1988) 1330.
[121] R.E. Walstedt and W.W. Warren, Jr., Appl. Magn. Reson. 3 (1992) 469.
[122] G. Shirane, Physica C 185 (1991) 80;
M. Matsuda et al., Phys. Rev. B 49 (1994) 6958.
[123] M. Imada, J. Phys. Soc. Japan 62 (1993) 1105.
[124] P. Monthoux and D.J. Scalapino, Phys. Rev. B.
[125] P.A. Lee and N. Read, Phys. Rev. Lett. 58 (1987) 2692.
[126] R. Noack, S.R. White, and D.J. Scalapino, Phys. Rev. Lett. 73 (1994) 882; preprint.
[127] J.E. Hirsch, Phys. Rev. Lett. 54 (1985) 1317.
[128] Z. Fisk et al., Science, 239 (1988) 33.
[129] K. Miyake, S. Schmitt-Rink, and C.M. Varma, Phys. Rev. B 34 (1986) 6554.
[130] D.J. Scalapino, E. Loh, Jr., and J.E. Hirsch, Phys. Rev. B 34 (1986) 8190.
[131] D.J. Scalapino, in High Temperature Superconductors, D.U. Gubser and M. Schlüter, eds., MRS Symp. Proc., Vol. EA-11 (Materials Research Society, Pittsburgh, Pa. 1987) 35.
[132] N.E. Bickers, D.J. Scalapino and R.T. Scalettar, Internat. J. Mod. Phys. B 1 (1987) 687.
[133] D.R. Harshman et al., Phys. Rev. B 36, 2386 (1987), Phys. Rev. B 39 (1989) 851.
[134] L. Kruisin-Elbaum et al., Phys. Rev. Lett. 62 (1989) 217.
[135] C. Gros, R. Joynt and T.M. Rice, Z. Phys. B, 68 (1987) 425. See also H. Yokoyama and H. Shiba, J. Phys. Soc. Japan, 57 (1988) 2482.
[136] M. Inui, S. Doniach, P.J. Hirschfeld and A.E. Ruckenstein, Phys. Rev. B 37 (1988) 2320.
[137] G. Kotliar and J. Liu, Phys. Rev. B 38 (1988) 5142.
[138] Q.P. Li, B.E.C. Koltenbah and R. Joynt, Phys. Rev. B 48 (1993) 437.
[139] F.J. Ohkawa, J. Phys. Soc. Japan 56 (1987) 2267.
[140] F.J. Ohkawa and N. Matsumoto, preprint.
[141] I.E. Dzyaloshinskii, Zh. Eksp. Teor. Fiz. 93 (1987) 1487.
[142] H.J. Schulz, Europhys. Lett. 4 (1987) 609.
[143] I.E. Dzyaloshinskii and V.M. Yakovenko, Zh. Eksp. Teor. Fiz. 94 (1988) 344.
[144] J. Ruvalds, C.T. Rieck and A. Virosztek, preprint.
[145] J.R. Schrieffer, X.-G. Wen, and S.-C. Zhang, Phys. Rev. Lett. 60 (1988) 944; 61 (1988) 2814; Phys. Rev. B 39 (1989) 11663.
[146] A.P. Kampf and J.R. Schrieffer, Phys. Rev. B 41 (1990) 6399; B 42 (1990) 7967.
[147] D.M. Frenkel and W. Hanke, Phys. Rev. B 42 (1990) 6711.
[148] N.E. Bickers, D.J. Scalapino and S.R. White, Phys. Rev. Lett. 62 (1989) 961.
[149] N.E. Bickers and S.R. White, Phys. Rev. B 43 (1991) 8044.
[150] K. Yonemitsu, J. Phys. Soc. Japan 58 (1989) 4576.
[151] N. Bulut, D.J. Scalapino and S.R. White, Phys. Rev. B 47 (1993) 2742.
[152] T. Moriya and Y. Takahashi, J. Phys. Soc. Japan 60 (1991) 776.
[153] P. Monthoux, A. Balatsky and D. Pines, Phys. Rev. B 46 (1992) 14803;
P. Monthoux and D. Pines, Phys. Rev. B 47 (1993) 6069.
[154] T. Moriya, Y. Takahashi and K. Ueda, Physica C 185 (1991) 114.
[155] E. Kaxiras and E. Manosakis, Phys. Rev. B 38 (1988) 866.
[156] E. Dagotto, J. Riera, and A.P. Young, Phys. Rev. B 42 (1990) 2347.
[157] E. Dagotto and J. Riera, Phys. Rev. Lett. 70 (1993) 682;
E. Dagotto et al., Phys. Rev. B 49 (1994) 3548.
[158] M. Boninsegni and E. Manousakis, Phys. Rev. B 46 (1992) 560.
[159] E. Dagotto et al., Phys. Rev. B 45 (1992) 10741.
[160] W.O. Putikka, M.U. Luchini and T.M. Rice, Phys. Rev. Lett. 68 (1992) 538.
[161] D.J. Scalapino, in: Perspectives in Many-Particle Physics, R.A. Broglia, J.R. Schrieffer and P.F. Bortignon, eds. (North-Holland, 1994) 95.
[162] G. Dopf, J. Wagner, P. Dieterich, A. Muramatsu, et al., Helvetica Physica Acta 65 (1992) 257.
[163] S.R. White et al., Phys. Rev. B 39 (1989) 839; B 40 (1989) 506.
[164] N. Bulut, D.J. Scalapino and S.R. White, Phys. Rev. B 47 (1993) 6157.

[165] M. Beasley used this approach in a Colloquium on the question of d-wave pairing.
[166] J. Bardeen, L.N. Cooper and J.R. Schrieffer, Phys. Rev. 108 (1957) 1175.
[167] V.J. Emery, Synth. Met. 13 (1986) 21.
[168] P.G. Radaelli et al., Phys. Rev. B 49 (1994) 4163.
[169] H. Takagi, et al., Phys. Rev. Lett. 68 (1992) 3777.
[170] C. Almasan and M.B. Maple, in: Chemistry of High Temperature Superconductors, C.N.R. Rao, ed. (World Scientific, Singapore 1991).

Note added in proof

The introduction should have noted that P.H. Dickinson and S. Doniach, Phys. Rev. B 47 (1993) 11447, have used a large-N expansion to study a three-band model and find a gap characterized by d-wave pairing of Cu–Cu holes and Cu–O holes with a relative phase of $\pi/2$ between the Cu–Cu and Cu–O pairs. They have called this $d+idp$ pairing. Likewise, our discussion of vertex corrections should contain a reference to A.J. Millis, Phys. Rev. B 45 (1992) 13047. In this paper he discusses vertex corrections and the Migdal theorem for a nearly antiferromagnetic Fermi liquid. Relevant to the discussion of neutron scattering, T.R. Thurston et al. [115] have argued that their neutron scattering data on $La_{1.85}Sr_{0.15}CuO_4$ excludes a conventional s-wave gap but could be compatible with a $d_{x^2-y^2}$-wave description. Also important for the discussion of the spin fluctuation spectral weight and T_c, M. Matsuda et al., Phys. Rev. B 49 (1994) 6958, have found that at intermediate energies the spin fluctuation strength of $La_{1.85}Sr_{0.15}CuO_4$ is a factor of 3 larger than that in $La_{1.98}Sr_{0.02}CuO_4$. Finally, we note two recent preprints on the relative phase of the gap. J.R. Kirtly et al. have recently carried out further studies of flux quantization in specially oriented tricrystal $YBa_2Cu_3O_{7-\delta}$ rings wich rule out the spin-flip scattering mechanism and support the idea that the 1/2-integer flux quantization is associated with the symmetry of the order parameter. A. Mathai et al. have used a SQUID microscope and a time-reversal test to study YBCO–Pb films in a similar geometry to that of Wollman et al. [95]. They have concluded that the pairing symmetry has a $d_{x^2-y^2}$ component and is invariant under time reversal.